POLITECNICO DI MILANO

SCHOOL OF INDUSTRIAL AND INFORMATION ENGINEERING

Master of Science in Automation and Control Engineering

Motion Control of Paramagnetic Microparticles

Supervisor: Prof. Paolo ROCCO

Co-supervisor: Prof. Sarthak MISRA

Tutors: Dr. Alper DANESI

Dr. Stefano SCHEGGI

Author:

Nicole FASIELLO

Id. number 818967

Academic Year 2015/2016

To my family

"Color my life with the chaos of troubles"

-The Boy with the Arab Strap-

Abstract

The application of microrobotics to the health care opens up the horizon for minimally invasive procedures, extremely targeted and highly precise with high benefits in terms of recovery time and healing of injury tissue. Magnetic technology has the potential to wirelessly actuate and control biological system, such as paramagnetic microparticles, which have the ability to navigate in fluids.

In this regard, this work presents a motion control for paramagnetic microparticles. A model of the overall magnetic system has been developed according to the experimental setup and the paramagnetic microparticle. The motion control is accomplished by a linear position/force controller and a nonlinear map. An optimisation algorithm has been implemented for the force-to-current map. Furthermore, the control has been extended to multiple numbers of robots by adopting a master-slave configuration, as a preliminary study of formation control. Simulation results are provided for evaluating the performance of the designed control.

Keywords: *Micro-robotics, Robotics in medicine, Magnetic actuators, Formation control*

Sommario

Da vent'anni a questa parte, la scienza della microrobotica ha allargato il suo campo di applicazione alla medicina. Ciò ha reso possibile interventi minimamente invasivi e di alta precisione, con notevoli vantaggi in termini di tempi di recupero e guarigione dei tessuti lesioniati. Infatti, grazie alle caratteristiche dei microrobots, è possibile operare interventi all' interno del corpo umano mirati a ridurre al minimo l'invasività e con essa i tempi di recupero. Molte malattie, come il cancro, necessitano di trattamenti localizzati; per questo motivo, il controllo di piccoli robots in grado di navigare all'interno dell'organismo e operare direttamente sul problema, rilasciando l'antidoto in loco, è diventato oggetto di molte ricerche.
Questa tesi presenta uno studio mirato alla realizzazione di un controllo del moto di microparticelle paramagnetiche, che possono essere attuate e controllate esternamente tramite un campo magnetico globale. A tal fine, si è sviluppato un modello del sistema che include la dinamica della microparticella e il sistema magnetico per il particolare setup Mobimag del Laboratorio di Chirurgia Robotica, presso l'Università di Twente, in Olanda. A causa della relazione che lega la forza magnetica alla corrente che alimenta le bobine, il sistema è non lineare. Una linearizzazione di tipo Input/Output ha reso possibile rincondurre il problema del controllo alla progettazione di un controllore lineare con retroazione di stato, utilizzando l'assegnamento degli autovalori. In seguito, è stato progettato un algoritmo di ottimizzazione per identificare la mappa non lineare che descrive la relazione fra forza e corrente. Successivamente, Il controllo è stato esteso a più particelle, adottando una configurazione di tipo master-slave per un controllo di formazione. Infine, le prestazioni del sistema sono state valutate tramite risultati di simulazione.

Parole chiavi: *Micro-robotica, Robotica in medicina, Attuatori magnetici, Controllo di formazione*

CONTENTS

Chapter 1 Introduction 17

Chapter 2 Structure of the Thesis Errore. Il segnalibro non è definito.

Chapter 3 State of the art 21

3.1 Microrobots 21

3.2 Actuation Methods and Control 22

Chapter 4 System Model 27

4.1 Paramagnetic Microparticle 27

4.1.1 Magnetic Force 27

4.1.2 Motion Dynamics 29

4.2 Mobimag Setup 30

4.3 State Space Model 37

Chapter 5 Motion Control of Microparticles 39

5.1 Design of Formation Control Law 41

5.1.1 Tracking control of a single microparticle 41

5.1.2 Master and Slave Tracking Control 44

5.1.3 Formation Control 47

5.2 Simulation 50

5.2.1 Motion Control of Single Microparticles 50

5.2.2 Formation Control 52

Chapter 6 Force-to-Current Map 57

6.1 One Particle: Comparison of the Analytical and Optimisation Methods 58

6.1.1 M.A. Method 58

6.1.2 Optimization Algorithm 60

6.1.3 Evaluation procedure of the M.A and Optimization approaches 61

6.2 GHP Algorithm applied to Two Particles case 62

6.3 Simulation 64

Chapter 7 Conclusion and Future works 71

List Of Tables

Table 1- Paramagnetic microparticle parameters.....29
Table 2- Mean square error (MSE) and R-square indices of fitting surfaces of the magnetic fields.....33
Table 3. Gain parameters for motion control of a single microparticle 50
Table 4. Initial conditions of the three microparticles 53
Table 5. Minimum, maximum and mean values of the absolute errors related to the component of the magnetic forces in x and y-direction. The values have been computed for the three techniques.....65

List Of Figures

Figure 1-Paramagnetic microparticle is immersed in a petri dish of 46 x 46 mm², containing water 30
Figure 2-Mobi-Mag device for medical l microrobots 31
Figure 3- FEM magnetic field data of $B1xp$ generated by the electromagnet 1 34
Figure 4- Fitting surface $FF1,x(p)$ of the current-to-field matrix $B1xp$ 34
Figure 5- FEM magnetic field data of $B1yp$ generated by the electromagnet 1 35
Figure 6- Fitting surface $FF1,x(p)$ of the current-to-field matrix $B1xp$ 35
Figure 7-FEM analysis of the norm(||B||). The coil is fed by a current of 1 A 36
Figure 8- norm(||B||) obtained with selected fitting functions 36
Figure 9-Block structure of the microparticle-magnetic field system. In green, the nonlinearity of the whole system is underlined 40
Figure 10-Nonlinear control developed with the input-output linearization technique 40
Figure 11-Control scheme of the motion controller for one particle 43
Figure 12-Control scheme of the master-slave control for two microparticles 47
Figure 13-Formation control scheme of multiple microrobots 49
Figure 14-Response time of the system for a step provided as signal input. On the top, it is shown the x vs time response, and the bottom y vs time . 51
Figure 15- Response time of the system for a sinusoidal reference. X- time response (on the top), Y-time (middle figure) and X-Y plane (on the bottom) 52
Figure 16-Master-Slave control of three microparticles for a sinusoidal signal 53
Figure 17-Time response of the formation errors, $ex1$(17.a) and $ey1(17.b)$, of the first slave along x and y direction 54

Figure 18-Time response of the formation errors, $ex2$(18.a) and $ey2$(18.b), of the second slave along x and y direction.....55
Figure 19-General logic to evaluate the accuracy of the inversion approaches proposed 62
Figure 20-Inverse Mapping for two microparticles.....63
Figure 21-Norm of the magnetic force computed by the simulation model (21.a), GHA algorithm (21.b), GHP algorithm (21.c), M.A method (21.d) .66
Figure 22- x-component of the magnetic force computed by the simulation model (22.a), GHA algorithm (22.b), GHP algorithm (22.c) 67
Figure 23- Response time of the system for a constant reference trajectory in x direction..... 68
Figure 24- Response time of the system for a constant reference trajectory in y direction.....69
Figure 25- Response time of the four currents during the tracking trajectory control.....70

Chapter 1
INTRODUCTION

Technological innovation has always played an important role in the world of medicine. In the last decade, the manipulation of micro-scale objects, in particular, has attracted growing attention for its numerous applications in health care and bioengineering [1]. Due to their micro-scale size, these objects can access complex and small regions of the human body, which up to now have been unreachable by any current medical device technology. Navigation control applied in the vascular network is a great challenge, as it consists of almost 100,000 km of blood vessels [2, 3], with diameters in the range of only a few millimetres [4].

The embrace of microrobotics in medicine has allowed procedures such as minimally invasive surgery and targeted drug delivery, which can drastically reduce recovery time, injury to tissue and increase the precision of the intervention. For instance, [5] studies the drug delivery for cancers applications. Although cancers are initially confined to a single region, they are presently still treated by chemotherapy, which does not distinguish between cancerous and healthy cells and entails the continuous injection of an excessive amount of toxic agents also into untargeted healthy organs. In this sense, medical microrobotics can represent the cure, as a targeted therapy is able to increase the concentration of therapeutics directly in loco, while preventing

unintentional damage to healthy tissue. Indeed, these small-scale untethered mobile robots are made of synthetic (i.e. magnetic materials, silicon, composites, elastomers) or biohybrid (integrated with muscle cells such as bacteria, spermatozoids and protozoa) materials and have the ability of self-propulsion. Medical microrobotics investigates the applicability of these objects in the area of medicine and , in particular, how they can assist and carry out tasks useful for medical procedures [6].

This work presents a motion control for paramagnetic microparticles, which are driven by an externally actuated magnetic field. A model representing the nonlinear system, including the paramagnetic dynamics and the magnetic system suite on the experimental setup is derived. Thanks to an input/output linearization it is possible to simplify the control problem into a linear control and force-to-current map, which resolves the complexity of dealing with nonlinear systems. The position-force controller has been designed through a pole-placement technique. Furthermore, the control has been extended to multiple numbers of robots by adopting a master-slave configuration, as a preliminary study of formation control. An optimisation algorithm for the derivation of a correct force-to-current map is proposed and compared with an analytical method discussed in literature. Simulation results demonstrate the effectiveness of the proposed motion controller for single microparticles, and highlight the remaining challenges in formation control of multiple particles.

The thesis is structured as follow: In Chapter 2 the research topics is introduced, presenting a survey of the existing works regarding microrobots and the applied controls. Chapter 3 describes the system model including the equations of motion which lead a paramagnetic microparticle along a fluid. In Chapter 4 a model-based control has been

designed using the pole-placement technique. The motion control has, then, been extended to multiple microrobots by adopting a master-slave configuration. Chapter 5 deals with the force-to-current providing an optimisation algorithm and comparing with an analytical approach devised in the literature. Finally, Chapter 6 summarise the results accomplished in this research, sketching the possible future works. Simulation results are shown at the end of each chapter.

This research has been carried out during a stay of the author in the Surgical Robotics Laboratory of the University of Twente, in the Netherlands.

Chapter 2

STATE OF THE ART

In order to define the topic of this research and offer a better understanding to the reader about the problem that will be tackled, a literature review is provided. This section will deal with the general knowledge of microrobotics, describing the characteristics of the considered objects and the different ways of actuation and control.

2.1 Microrobots

In recent years we have witnessed enormous advances in the field of microrobotics. This started from an increased use of microelectromechanical systems (MEMS) since the 1990s. Advances in micro – and nanoscale science and technology, together with increasing demand of microsystems for application in medicine, biotechnology, manufacturing, and mobile sensor networks, has led to the development of tiny mobile robots that could access enclosed small spaces down to the micron scale such as inside the human body and microfluidic devices and could manipulate and interact with micro/nanoscale entities. Microrobots have the potential to revolutionise many aspects of medicine, biology and manufacturing. For example, in the medical domain, they might have high-impact applications such as minimally invasive diagnosis and treatment, drug delivery and non-invasive surgery [6]. Two main characteristics are

needed by microsystems to perform these novel tasks with high efficiency: very small size microrobots and multi-robot control. The principles governing the design of such submillimeter scale robots rely on an understanding of microscale physics, fabrication, and novel control strategies.

There is no standardised definition of the term microrobot. In fact, reported microrobots range in size from single μms to the cm scale. However, one common approach defines a microrobot as existing in the size range of hundreds of nm to 1 mm. In some cases, component size scale being micron scale is taken as the crucial aspect, which could then include millimetre or centimeter-scale mobile robots as microrobots. In other cases, overall size scale being micron scale is emphasised where mobile robots able to fit in spaces smaller than a millimetre are considered as microrobots. A more relevant definition might involve the types of physical interactions which dominate the motion and interaction of the robot. Large or centi/milli-scale robots are dominated by inertial and other bulk forces. As we go smaller, the balance of different forces changes dramatically, and we see increases in friction and adhesion while the influence of weight and inertia is markedly reduced [7]. The lower-bound of microrobots could likewise be when assumptions of the continuity of matter are no longer valid. At sizes below tens of μm, effects such as Brownian motion and chemical interactions could lead to stochastic descriptions of motion behaviour. These physical effects must be taken into account when designing and operating robots at the small scale.

2.2 Actuation Methods and Control

The actuation and control of microrobots present two challenges:

1- The very small size which does not allow the use of on-board power and control
2- The microscale physical effects which do not allow the use of inertial-based actuators

The implications of the aforementioned challenges led to remote control exploiting different physical aspects. Magnetic actuation is widely used for remote microrobot control of size 150 to 250 μm. Due to their ability to penetrate most materials (including biological materials), magnetic fields are naturally suited to control microscale objects in remote, inaccessible spaces. Moreover, magnetic forces and torques can be relatively strong with compact system size and low hardware cost. For this kind of actuation permanent magnetic, ferromagnetic or paramagnetic materials are integrated into the microrobots fabrication, thus the robots experience a magnetic force and a torque due to the electromagnetic field [8].
By controlling both the magnetic field and its gradients in the microrobot workspace, it is possible to provide independent magnetic torques and forces, realising autonomous navigation.
Magnetic fields can be supplied by magnetic coils or by large permanent magnets outside the microrobot workspace. Magnetic coils have the major advantage that they can deliver varying fields with no moving parts, and can be designed in a variety of ways to create spatially uniform magnetic fields and gradients. Permanent magnets, however, can provide large fields without the use of large electrical currents. The field, in this case, can be modulated by translating or rotating one or more external magnets, but in general cannot be turned off without moving the external magnets far from the workspace.

Magnetic actuation by MRI

Magnetic actuation using a clinical MRI machine could leverage existing equipment infrastructure for navigating magnetic microrobots inside the human body. Clinical MRI systems are designed for imaging and thus have several limitations for the propulsion of magnetic microrobots. Unlike the magnetic coil systems which can control the coil currents in each coil independently, an MRI machine provides a static field down the length of

the system. This static field is provided by large superconducting magnets, and typically can be 1.5 T or higher, especially in MRI systems used for research. For imaging, magnetic field gradients up to ~40 mT/m can be created in any direction. These gradients can be used for microrobot propulsion by gradient pulling, and can potentially be increased through custom coil installations. This is the case of the nanorobotic platform for in-vivo navigation realised by Sylvain et al. [9]. They exploited an MRI system to lead untethered devices to a target region in the blood vessel that is too narrow to be reached by catheterization. The three imaging gradient coils of the MRI system are utilized to provide actuation force for the ferromagnetic microrobots [10], since the magnetic gradient was not sufficient to precisely reach a particular region, the researchers proposed three additional special gradient coils that can be installed along with the existing gradient coils to provide enough actuation to reach the target region. This system allows to control a swarm of magnetic carriers towards a region inside a body, however, it cannot provide independent control of the microrobots. It remains a quite used actuation method to provide targeted drug delivery and noninvasive therapy.

Magnetic field by coils

In coils configurations, the magnetic field generated depends on the current flowing through the coil. The control input is the voltage on the coil, and the current can be sensed using Hall effect current sensors if precise feedback control is required. In particular, the spatial flexibility of coils configurations does allow an increased level of controllable microrobots. An example of special coil configuration is the work of Pawashe et al. [11], that have developed a magnetic actuation system which consists of six orthogonal magnetic coils. The work-space is located at the intersection of the axes of all the coil and the microrobots respond to the magnetic force generated by the magnetic coils and navigate towards the direction of the resultant force.

For all actuation methods, the critical point is the independent multi micro-robot control. Several methods to achieve this objective have been explored. Various groups have achieved independent control by introducing heterogeneity in the microrobots so that they can respond differently to the same control input. Among these solutions we report Diller et al. [12], who achieved a different response of three microrobots to the global magnetic field navigating them to three different goal locations. Cheang et al. [13] developed a team of microswimmers made of magnetic microparticles that are geometrically similar but magnetically different so that they exhibit different swimming behaviours to the same global rotating magnetic field.
Others researchers focused on the design and implementation of the setup. Cappelleri et al. [14] have developed a setup made of 64 micro-coils arrays which can generate a local magnetic field for independent actuation of multiple robots. Torres et al. have presented a novel method of actuation for swarm control of multiple untethered microrobots with a global magnetic field generated by a single conical permanent magnet [15]. These solutions present some weak points, starting from the non-homogeneity of the micro-robots, up to inaccurate setup.

This work discusses a promising approach, which exploits utilisation of magnetic coils such that a uniform magnetic field is obtained along the workspace. As the microparticles do not have heterogeneity, the synchronisation between their motion has been developed by designing a suitable control law.

Chapter 3
SYSTEM MODEL

This section describes the basic principles of the implemented non-linear model, including the paramagnetic microparticle dynamics and the magnetic system for the particular experimental setup provided by the University of Twente.
First, the physical laws due to the material properties of these micro-agents are studied, investigating how they interact with a magnetic field. Secondly, the magnetic system interesting the workspace is analysed and the characteristic parameters are identified. Finally, in the last section, the two models are integrated and expressed in state-space representation.

3.1 Paramagnetic Microparticle

3.1.1 Magnetic Force

The microrobots considered for this research are paramagnetic spherical microparticles (e.g, diameters around 100 μm, Figure 1) made of iron-oxide in a polylactic acid matrix (PLA-Particles-M-redF-plain from Micromod Partikeltechnologie GmbH, Rostock-Warnemuende, Germany). Thanks to properties due to their material, these objects are self-propelled and can be wirelessly controlled. The microparticles are off-board actuated through the magnetic field gradient, generated by the external electromagnets.

The micro-agents immersed in a magnetic field experience a magnetic force [16]. Let $p = [x\ y\ z]^T \in \mathbb{R}^{3\times1}$ be the position of the microparticle in the 3D space. $\vec{m} \in \mathbb{R}^{3\times1}$ and $\vec{B} \in \mathbb{R}^{3\times1}$ represent respectively the magnetic dipole and the magnetic field at the point p. The exerted force can be defined as:

$$F(p) = (m(p) \cdot \nabla)B(p) \tag{1}$$

where $(p) = \begin{bmatrix} F_x & F_y & F_z \end{bmatrix}^T \in \mathbb{R}^{3\times1}$. As the electric current flowing through the workspace is null, for Maxwell's equations $\nabla \times B = 0$. Therefore (1) can be expressed as

$$F(p) = \begin{pmatrix} \frac{\partial B(p)}{\partial x} & \frac{\partial B(p)}{\partial y} & \frac{\partial B(p)}{\partial z} \end{pmatrix}^T m(p) \tag{2}$$

In [8] the magnetic moment is computed by the volume integral of the induced magnetisation $M(p)$

$$m(p) = \int_V M(p)dV = \frac{4}{3}\pi r_p^3 M(p) \tag{3}$$

where V and r_p are the volume and the radius of the spherical particle. The magnetization of the microparticle is related to the magnetic field strength ($H(p) \in \mathbb{R}^{3\times1}$) by the equation $M(p) = \chi_m H(p)$, where χ_m is the magnetic susceptibility constant. $B(p)$ can be expressed in terms of magnetic field strength as $B(p) = \mu H(p)$, where μ is the permeability coefficient given by $\mu = \mu_0(1 + \chi_m)$, while μ_0 is the vacuum permeability equal to $4\pi\ x\ 10^{-7} T \cdot m/A$. Thus (3) can be rewritten as

$$m(p) = \frac{4}{3}\pi r_p^3 \chi_m H(p) = \frac{1}{\mu}\frac{4}{3}\pi r_p^3 \chi_m B(p) \tag{4}$$

Assuming intrinsic isotropic properties and spherical geometry of the studied microparticles, these are subjected to pure forces and zero magnetic torque [17]. Substituting (4) in equation (1), the magnetic force exerted on a microparticle and responsible for the translational displacement, can be expressed as a function of the magnetic field

$$F(p) = \frac{1}{\mu}\frac{4}{3}\pi r_p^3 \chi_m \nabla(B(p)^T B(p)) \quad (5)$$

3.1.2 Motion Dynamics

Paramagnetic microparticles can navigate through a fluid under the influence of the magnetic forces. During the motion the particle experiences drag force $F_d(\dot{p}) \in \mathbb{R}^{3\times1}$ and buoyancy force $F_b \in \mathbb{R}^{3\times1}$.

$$F(p) + F_d(\dot{p}) + F_b = M_p\ddot{p} \quad (6)$$

The motion dynamics of the particle of mass M_p , navigating in the fluid is given in equation (6). The Buoyancy force acts only on the z-direction and it is defined as $F_b = [0\ 0\ V(\rho_b - \rho_w)g]^T$, where ρ_b and ρ_w are the density of the microparticle and the fluid respectively, while g is the gravity acceleration.

Parameter	Value	Parameter	Value
r_p [μm]	50	ρ_b [Kgm^{-3}]	1.4×10^3
χ_m	0.075	ρ_w [Kgm^{-3}]	998.2
M_p [Kg]	7.33×10^{-10}	η [mPa.s]	1.0

Table 1- Paramagnetic microparticle parameters

The drag coefficient is related to the flow type. Equation (7) computes the Reynolds number, which is the dimensionless quantity that embodies the interaction between a fluid's inertia and viscosity as it flows around an object.

$$Re = \frac{2\rho_w \dot{p} r_p}{\eta} \quad (7)$$

where η is the dynamic viscosity of the fluid.

Assuming the maximum velocity $\dot{p}$ of the microparticle to be 1 [mms^{-1}], the Re is estimated to be less than 0.1, i.e. laminar flow. Thus the drag force has the same direction of the fluid flow and is given by the Stoke's law [18] :

$$F_{d(\dot{p})} = -\alpha\dot{p} = -6\pi\eta r_p\dot{p} \quad (8)$$

From now on, the study will focus only in two dimensions, in particular, the x-y plane.

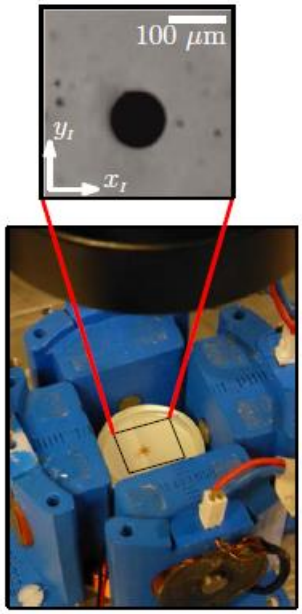

Figure 1-Paramagnetic microparticle is immersed in a petri dish of 46 x 46 mm², containing water

3.2 Mobimag Setup

Mobimag is a compact device, developed at the University of Twente (Enschede, Netherlands), for medical research, which allows studying wireless control of magnetic microrobots. It consists of 6 electromagnetic coils with iron cores placed orthogonally around the region of interest (Figure 2).

Each coil is powered by an Elmo 'Whistle' 1/60 DC servo drive (Elmo Motion Control, Petach-Tikva, Israel). A Blackfly 1.4 MP Color GigE PoE (Point Grey Research Inc., Richmond, Canada) camera is mounted on a Mitutoyo FS70 microscope unit (Mitutoyo, Kawasaki, Japan) using a Mitutoyo M Plan Apo2 / 0.055 Objective.

A COMSOL Multiphysics model (COMSOL Inc., Burlington, USA) was developed by our research group [19] in order to optimise the dimensions of the coils. These were designed to guarantee that a magnetic field intensity of 10 mT is generated in the middle point of the workspace, whenever the current in one of the coils is set to 1A.

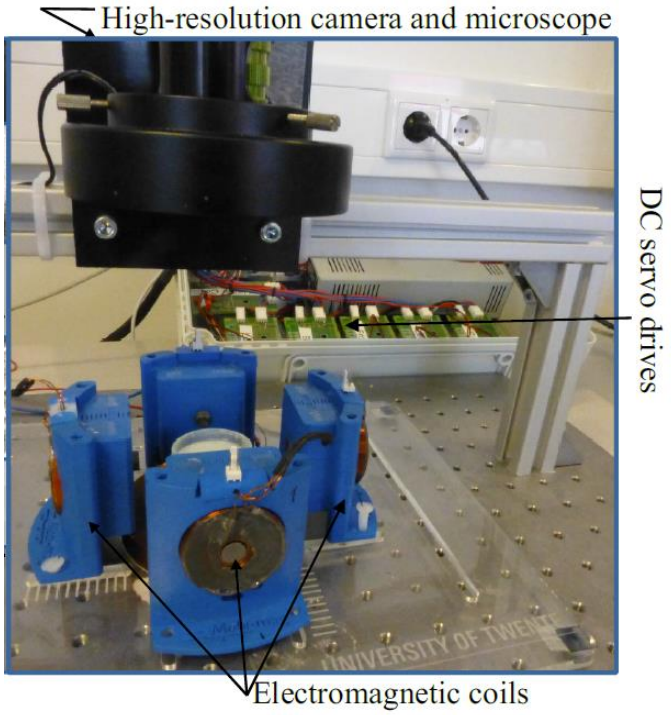

Figure 2-Mobi-Mag device for medical l microrobots

Due to the single camera system, the z-direction was not possible to track. Thus, the bottom and top coils were not taken into account in this research. As the four coils are fed by the four currents $I = [I_1\, I_2\, I_3\, I_4]^T \in \mathbb{R}^{4\times1}$, a magnetic field is generated in the workspace. Due to the material properties, the microparticles immersed in the magnetic field are subjected to magnetic forces, which can control their motion. Let $B_i(p) \in \mathbb{R}^{2\times1}$ be the magnetic flux density generated by the coil i at a position p with respect the global frame, the overall magnetic field along the x and y-directions can be computed by the superposition [16] of the contribution of the i^{th} electromagnets as

$$B(p) = \sum_{i=1}^{n} B_i(p) \tag{9}$$

where $n = 4$ is the number of air-core electromagnets. In the considered workspace the current is assumed to vary linearly with magnetic field. Therefore (9) can be expressed as

$$B(p) = \sum_{i=1}^{n} \tilde{B}_i(p) I_i = \tilde{B}(p) I \tag{10}$$

where $\tilde{B}(p) = \begin{bmatrix} \tilde{B}_x(p) \\ \tilde{B}_y(p) \end{bmatrix} \in \mathbb{R}^{2\times n}$ represents the position-dependent matrix of the magnetic field evaluated at position p. The component elements of $\tilde{B}(p)$ matrix depend on parameters and the number of the coils. A FEM analysis has been carried out in order to evaluate the current-to-field map $\tilde{B}(p)$. The analysis has been validated in [20] by comparing the magnetic field data obtained with the measured one, including the related uncertainties.

Being able to evaluate the magnetic field in each position of the workspace is a necessary condition to control the motion of the microrobots, as it is strictly related to the magnetic field. For this reason, the current-to-field map has been fitted using the data provided by the FEM analysis. After different attempts, a 5th order polynomial was chosen as fitting function. A higher order polynomial would not have gained a lot more in terms of accuracy against computational time.

Figure 4 andFigure 6 show the two surfaces obtained by fitting the COMSOL data (Figure 3 and Figure 5). The model has been evaluated through a preliminary study on the goodness of the fit (Table 2).

	MSE	R-square
$\mathbf{B_x}$	1.9221×10^{-5}	0.9560
$\mathbf{B_y}$	9.9761×10^{-6}	0.9091
$\|\|\boldsymbol{B}\|\|$	1.4013×10^{-5}	0.9743

Table 2- Mean square error (MSE) and R-square indices of fitting surfaces of the magnetic fields

According to the radius of the Petri dish (15 mm²), which hosts the microparticle, the workspace analysed for the magnetic field fitting has been shrunk to a 35×35 [mm²] square, improving the approximation of the fitting surface. Figure 7 and Figure 8 show the norms of the magnetic fields data and the one obtained through the fitting technique.

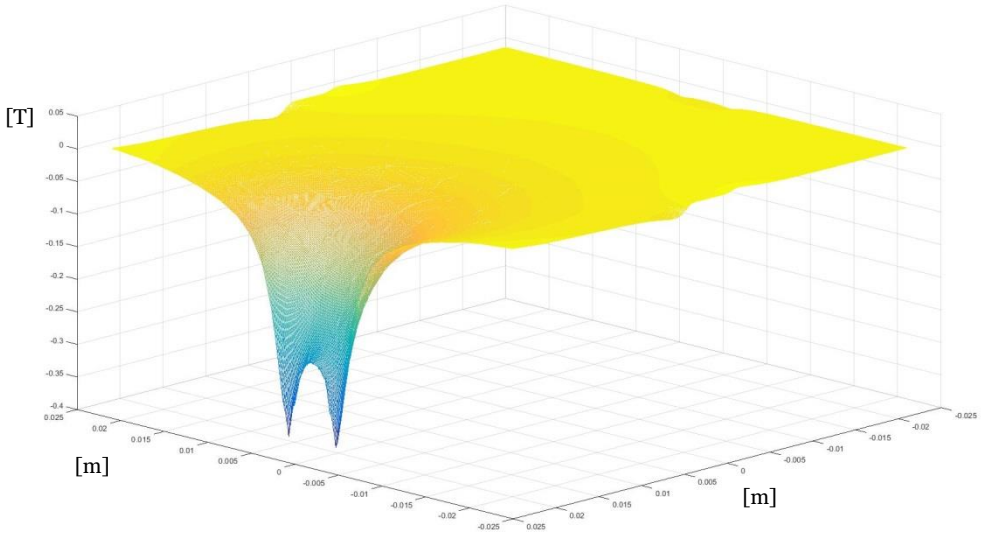

Figure 3- FEM magnetic field data of $\tilde{B}_{1x}(p)$ generated by the electromagnet 1

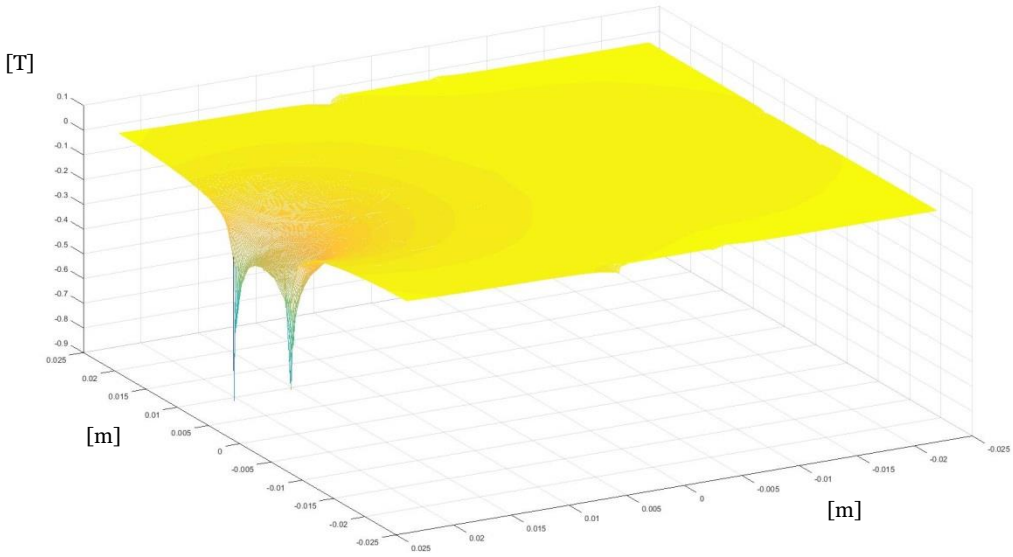

Figure 4- Fitting surface $FF_{1,x}(p)$ of the current-to-field matrix $\tilde{B}_{1x}(p)$

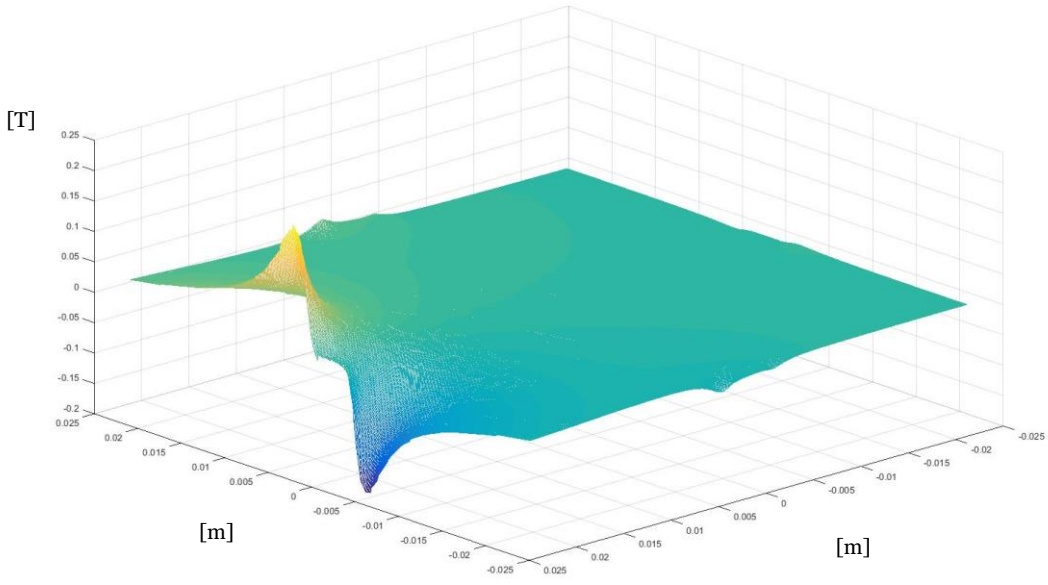

Figure 5- FEM magnetic field data of $\tilde{B}_{1y}(p)$ generated by the electromagnet 1

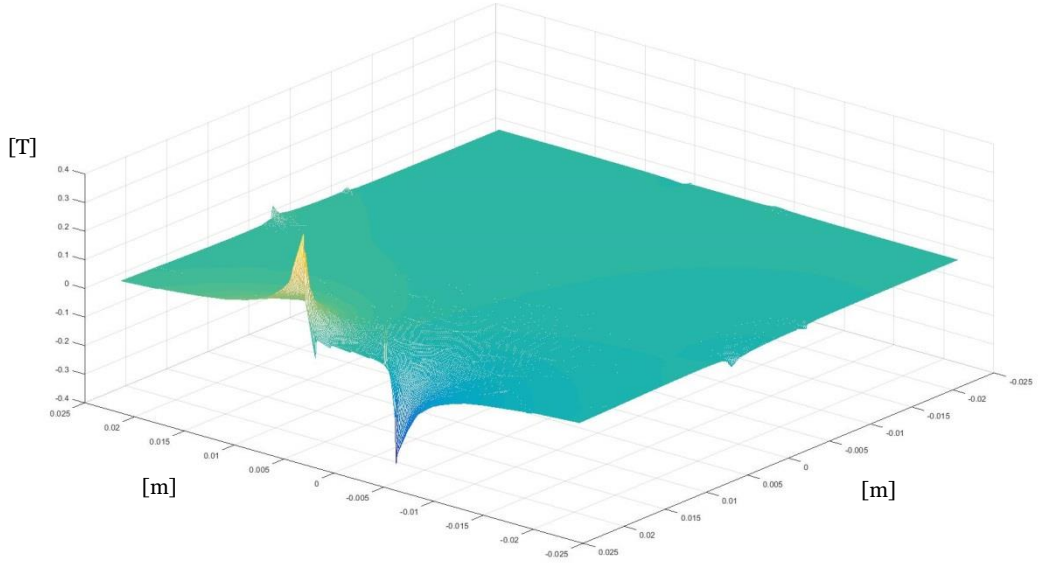

Figure 6- Fitting surface $FF_{1,x}(p)$ of the current-to-field matrix $\tilde{B}_{1x}(p)$

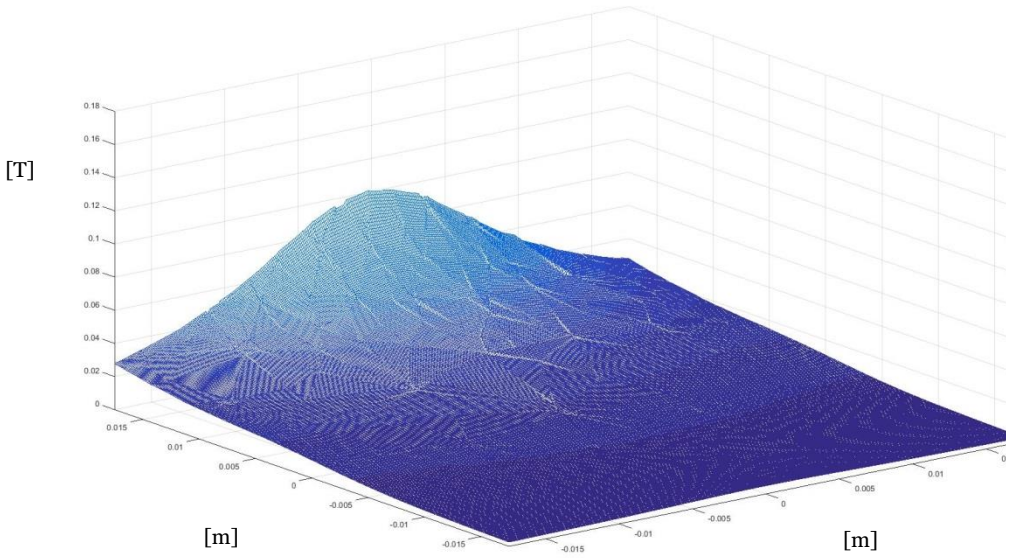

Figure 7-FEM analysis of the norm(||B||). The coil is fed by a current of 1 A

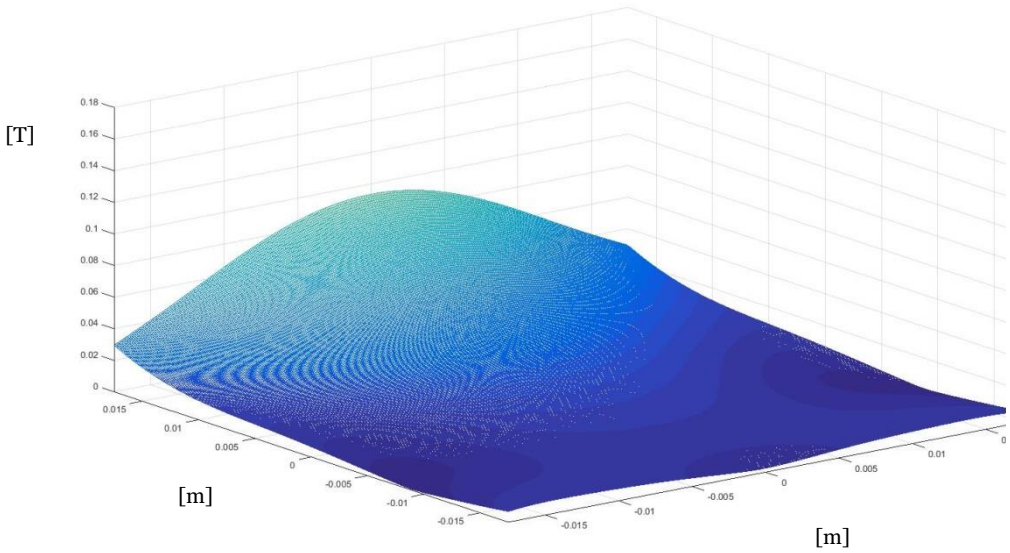

Figure 8- norm(||B||) obtained with selected fitting functions

As already mentioned before, $\tilde{B}(p)$ is obtained by imposing the contribution of the single coil. Equation (11) reports the expression of the fitted magnetic field for respectively along the x and the y direction respectively induced by the i_{th} electromagnet.

$$\begin{aligned} FF_{i,x}(x,y) = \; & p_{00,i,x} + p_{10,i,x}x + p_{01,i,x}y + p_{20,i,x}x^2 + p_{11,i,x}xy \\ & + p_{02,i,x}y^2 + p_{30,i,x}x^3 + p_{21,i,x}x^2y + p_{12,i,x}xy^2 \\ & + p_{03,i,x}y^3 + p_{40,i,x}x^4 + p_{31,i,x}x^3y + p_{22,i,x}x^2y^2 \\ & + p_{13,i,x}xy^3 + p_{04,i,x}y^4 + p_{50,i,x}x^5 + p_{41,i,x}x^4y \\ & + p_{32,i,x}x^3y^2 + p_{23,i,x}x^2y^3 + p_{14,i,x}xy^4 \\ & + p_{05,i,y}x^5 \\ FF_{i,y}(x,y) = \; & p_{00,i,y} + p_{10,i,y}x + p_{01,i,y}y + p_{20,i,y}x^2 + p_{11,i,y}xy \\ & + p_{02,i,y}y^2 + p_{30,i,y}x^3 + p_{21,i,y}x^2y + p_{12,i,y}xy^2 \\ & + p_{03,i,y}y^3 + p_{40,i,y}x^4 + p_{31,i,y}x^3y + p_{22,i,y}x^2y^2 \\ & + p_{13,i,y}xy^3 + p_{04,i,y}y^4 + p_{50,i,y}x^5 + p_{41,i,y}x^4y \\ & + p_{32,i,y}x^3y^2 + p_{23,i,y}x^2y^3 + p_{14,i,y}xy^4 \\ & + p_{05,i,y}x^5 \end{aligned} \tag{11}$$

Equation (12) shows the structure of the position-dependent matrix $\tilde{B}(p)$.

$$\tilde{B}(p) = \begin{bmatrix} FF_{1,x}(p) & FF_{2,x}(p) & FF_{3,x}(p) & FF_{4,x}(p) \\ FF_{1,y}(p) & FF_{2,y}(p) & FF_{3,y}(p) & FF_{4,y}(p) \end{bmatrix} \tag{12}$$

3.3 State Space Model

The microparticle model described in section 3.1 has been rewritten in state-space representation. Let $p = [x \quad y]^T$ and $\dot{p} = [\dot{x} \quad \dot{y}]^T$ be the position and the velocity of the microparticle in the 2D space respectively. The continuous-time dynamics of the paramagnetic microparticle reported in eq.(6), including the drag force (eq.(8)), can be expressed as

$$\dot{\xi} = A\xi + Bf(p) = \begin{bmatrix} \dot{p} \\ \ddot{p} \end{bmatrix} = \begin{bmatrix} 0_{2\times2} & I_{2\times2} \\ 0_{2\times2} & \frac{\alpha}{M_p} I_{2\times2} \end{bmatrix} \begin{bmatrix} p \\ \dot{p} \end{bmatrix} + \begin{bmatrix} 0_{2\times2} \\ \frac{1}{M_p} I_{2\times2} \end{bmatrix} \begin{bmatrix} f_x(p) \\ f_y(p) \end{bmatrix} \quad (13)$$

where $f_x(p)$, $f_y(p)$ are the magnetic forces along the x and y directions, defined in (5).

(13) is a MIMO nonlinear system. Indeed, the nonlinearity is intrinsic in the control variable, which depends on the particle position p and presents a quadratic relation with respect to the current. As explained in section 3.2, Mobimag setup is controllable by current which is linear with respect to the magnetic field but not with respect to the magnetic force. By combining the (5) and (10) and considering the current position independent, the relation between the force and current is given by

$$F(p) = \beta I^T \nabla (\tilde{B}(p)^T \tilde{B}(p)) I \quad (14)$$

where β is the constant value equal to $\frac{1}{\mu} \frac{4}{3} \pi r_p^3 \chi_m$.

Chapter 4

MOTION CONTROL OF MICROPARTICLES

To address challenges as drug delivery and non-invasive surgery, it is necessary to develop a control able to handle a group of microrobots along a reference trajectory.

In Chapter 3 the model of the microparticle-magnetic field system has been described. These objects do not have any actuators on-board, indeed they are directly controllable through the magnetic forces due to the external magnetic field generated by the electromagnets set at four corners of the workspace. The control design problem is to determine the magnetic force which drives the particles along the desired trajectory.

Equation (14) points out the nonlinearity of the magnetic force against the position and the current vector. The intensity of the force drops with the distance from the coils and presents a quadratic relation with respect to the current.

Nonlinear systems present complex dynamics and they are difficult to control. For this reason, an input-output linearization approach has been applied for this study in order to find the equivalent linear system through a change of variables and control input. This technique, already discussed in the literature [21], 14], aims to find the inverse of the map between the transformed input F_m and the actual output I to get rid of the nonlinearity (Figure 9).

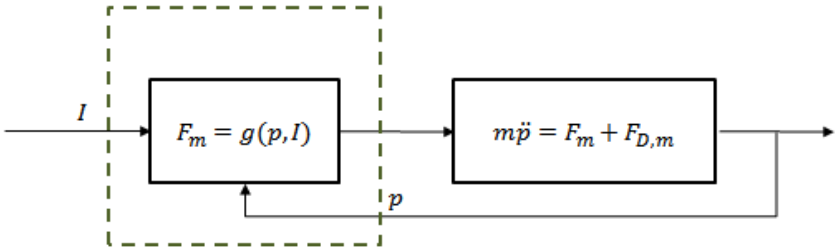

Figure 9-Block structure of the microparticle-magnetic field system. In green, the nonlinearity of the whole system is underlined

Chapter 5 will deal with a suitable inverse map $g^{-1}(\cdot) = \mathbb{R}^m \times \mathbb{R}^m \to \mathbb{R}^n$ defined as

$$g\left(p, g^{-1}(p, F_m)\right) = F_m \tag{15}$$

The nonlinear controller can then be split in a linear controller followed by the force-to-current map (15), which cancels out the nonlinearity block of the system (Figure 10).

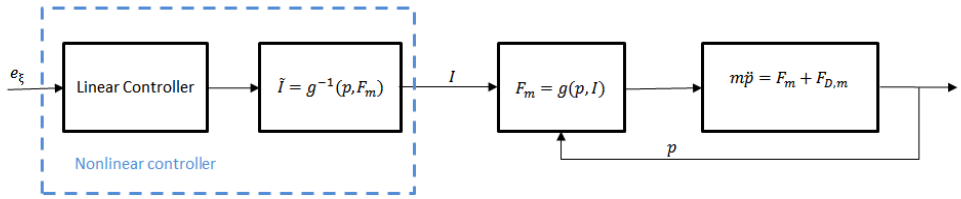

Figure 10-Nonlinear control developed with the input-output linearization technique

In this way, the closed-loop system can be simplified into a linear system defined by the state-space model defined in (13), when considering the magnetic forces as an input variable.

This section aims to design a formation control law for the particular case-study of the paramagnetic microparticle immersed in a magnetic field. Firstly, we focus on a tracking control for a single microparticle and then in Section 4.1.2 two microparticles are considered for the trajectory tracking

problem. Finally, the control law is extended to more microparticles for a preliminary study for formation control of a group of microparticles.

4.1 Design of Formation Control Law

4.1.1 Tracking control of a single microparticle

The motion control strategy is aimed at tracking a time-varying reference trajectory specified within the workspace.

Consider the dynamics of the microparticle, studied in section 3.1.2 :

$$\dot{\xi} = A\xi + B\mathrm{f}$$
$$y = \xi \tag{16}$$

we want to design a state feedback control law such that the output y track asymptotically a reference signal $p_{ref}(t) \in \mathbb{R}^{2\times 1}$, with its successive derivatives $\dot{p}_{ref}(t)$ and $\ddot{p}_{ref}(t)$ bounded for $t \geq 0$ and continuous function of t . $p_m(t), \dot{p}_m(t)\ and\ \ddot{p}_m(t)$ represent the position, velocity and acceleration of the microparticle at the time instant t.

Let

$$\mathcal{P} = \begin{bmatrix} p_{ref} \\ \dot{p}_{ref} \end{bmatrix},\ \varepsilon = \begin{bmatrix} p_{ref} - p_m \\ \dot{p}_{ref} - \dot{p}_m \end{bmatrix} = \mathcal{P} - \xi \in \mathbb{R}^4 \tag{17}$$

By applying a change of variables $\varepsilon = \mathcal{P} - \xi$ to (16), we obtain:

$$\dot{\varepsilon} = A\varepsilon - B\mathrm{f} - A\mathcal{P} + \dot{\mathcal{P}} \tag{18}$$

The computation of (18) yields:

$$\frac{d}{dt}\begin{bmatrix} p_{ref} - p_m \\ \dot{p}_{ref} - \dot{p}_m \end{bmatrix} = \begin{bmatrix} \dot{e}_{ref} \\ \ddot{p}_{ref} - \ddot{p}_m \end{bmatrix} = \begin{bmatrix} \dot{e}_{ref} \\ -\frac{F_{D,M}}{M_P} - \frac{\mathrm{f}}{\mathrm{M_P}} + \ddot{p}_{ref} \end{bmatrix} \tag{19}$$

The control problem consists of identifying a control input f that stabilises the system so that all closed-loop eigenvalues are placed in the left half of the complex plane.

Once verified the controllability of the system, a pole-placement technique [15, 16] has been used in order to achieve the stability of the closed-loop system.

Theorem 5.1 *Assuming that the pair (A, B) is controllable, there exists a feedback F such that the closed-loop system eigenvalues can be placed in arbitrary locations.*

The suitable control law in the form shown in (20).

$$\begin{aligned} \mathrm{f} &= F_{ref} - \hat{F}_{D,m} \\ &= -\hat{F}_{D,m} + K_P(p_{ref} - p_m) + K_D(\dot{p}_{ref} - \dot{p}_m) \\ &+ \widehat{M_P}\ddot{p}_{ref} \end{aligned} \tag{20}$$

where $\widehat{M}_P$ and $\hat{F}_{D,m}$ are the estimated mass of the particle and drag force, which we assumed to be equal to the real ones.

$$\begin{aligned} &\frac{d}{dt}\begin{bmatrix} p_{ref} - p_m \\ \dot{p}_{ref} - \dot{p}_m \end{bmatrix} = \begin{bmatrix} \dot{e}_{ref} \\ \ddot{p}_{ref} - \ddot{p}_m \end{bmatrix} \\ &= \begin{bmatrix} \dot{e}_{ref} \\ \ddot{p}_{ref} - \dfrac{1}{M_P}\left(K_P e_{ref} + K_D \dot{e}_{ref} + \hat{m}\ddot{p}_{ref} - \hat{F}_{D,m}\right) - F_{D,M} \end{bmatrix} \end{aligned} \tag{21}$$

The gain matrices $K_D = \begin{bmatrix} k_d & 0 \\ 0 & k_d \end{bmatrix}$ and $K_P = \begin{bmatrix} k_p & 0 \\ 0 & k_p \end{bmatrix}$, with k_d and k_p constant values $\in \mathbb{R}$, were chosen positive definite and in order to stabilize, according to the Hurwitz criterion [25], the closed-loop system, given by:

$$\ddot{e}_{ref} + \frac{K_D}{M_P}\dot{e}_{ref} + \frac{K_P}{M_P}e_{ref} = 0 \tag{22}$$

The trajectory tracking control scheme (shown in green Figure 11) is mainly composed of two feedback control loop, one proportional and one derivative. From the model of the system (13), it can be noted that the process itself already contains an integrator. For this reason, an integral action is highly discouraged in aid of the derivative contribution which adds phase lead, stabilising more the loop.

The feedforward contribution on the acceleration improves the performance of the control. Indeed, it estimates the output from the PD-control without waiting for its response. In this way, the error has kept smaller than relying only on the PD algorithm. The $\hat{F}_{D,m}$ compensate the disturbance given by the drag force acting on the particle [26].

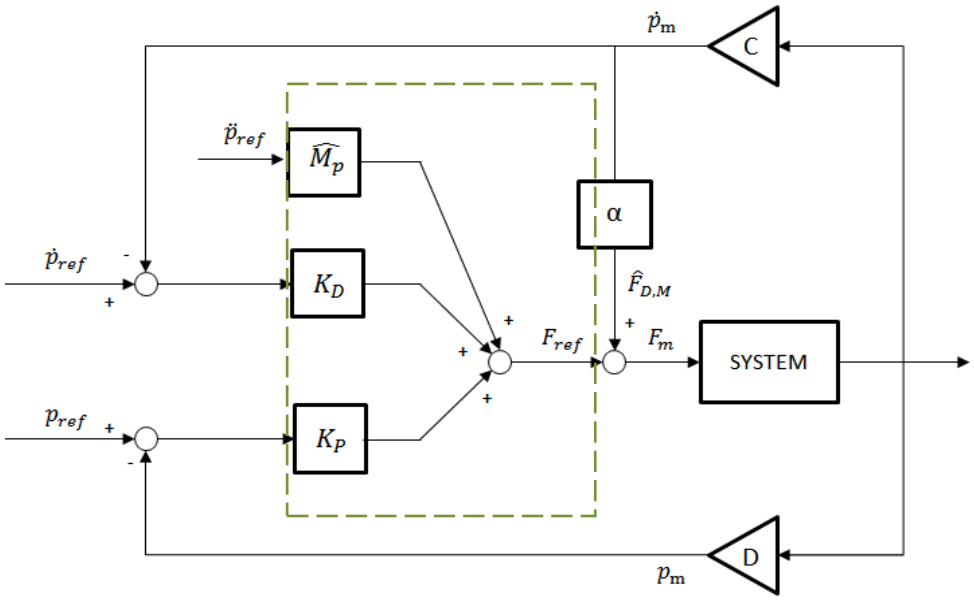

Figure 11-Control scheme of the motion controller for one particle

$C = \begin{bmatrix} 0 & 0 & 1 & 0 \\ 0 & 0 & 0 & 1 \end{bmatrix}$ and $D = \begin{bmatrix} 1 & 0 & 0 & 0 \\ 0 & 1 & 0 & 0 \end{bmatrix}$ represent respectively the constant matrices to decouple the position p_m and the velocity $\dot{p}_m$.

The system has been tested for different input signals and different initial conditions. The results are shown in section 4.1.1.

Once the reference tracking of the single particle is achieved, we proceeded by studying the two-particles system. For this control problem, a master-slave technique has been adopted.

4.1.2 Master and Slave Tracking Control

Njimeijer and Rodriguez-Angeles in [27] discuss the importance of the synchronisation in robotic systems for tasks that cannot be carried out by a single robot, as the case of drug delivery. According to [28], our case-study can be identified as external synchronisation. Assuming a multi-composed system, it is characterised by a more "powerful" object, which can boast an independent motion, in spite of the others robots. Master and slave approach represents only a configuration of this kind of synchronisation. More specifically, only the master has the information of the reference trajectory, while the slave follows the master motion. The key point of approach is that each particle becomes a master to one particle and the slave of another.

In the particular case-study analysed, master and slave do not have differences in the shape either in density, but they are all the same. The "Master" or the "Slave" titles are only due to the control law. Indeed, depending on how they are managed by the controller, they can lead or follow. As the roles are exchangeable and not fixed, this approach has the advantage that each particle can become a master to one particle and the slave of another one.

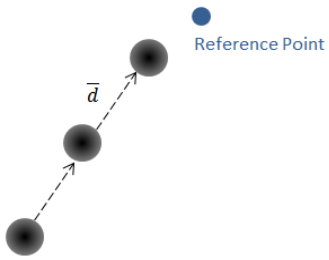

Figure 1-Master-Slave approach in straight line configuration

Initially, only two microrobots were considered in order to develop the individual tracking control of a slave.

The control law has been designed in a dual way of the one shown in section 4.1.1, based on the error dynamics. When setting up the master-slave control problem, it is necessary to define a formation parameter, which locks the slave to a fixed distance $d = \begin{bmatrix} d_x \\ d_y \end{bmatrix}$, to the master. The difference between the master and slave position, including the parameter d, is called *formation error*. When this error is zero, it means that the two particles are in formation, as the distance between these two is exactly equal to d. By computing the successive derivative of the formation error, an error dynamics can be determined.

$$\begin{cases} e = p_m - p_s - d \\ \dot{e} = \dot{p}_m - \dot{p}_s - \dot{d} \\ \ddot{e} = \ddot{p}_m - \ddot{p}_s - \ddot{d} \end{cases} \tag{23}$$

$\dot{d}$ and $\ddot{d}$ specify the difference between the two microrobots in terms of velocity and acceleration, respectively. As we want the two objects navigate at a set distance but with the same velocity and acceleration, no constraint has been imposed on the formation velocity and acceleration. According to that, a constant value was chosen for the formation parameter ($d_x = d_y = 8e^{-5}[m]$, when considering the radius of the particle), whilst the related derivative $\dot{d}$ and $\ddot{d}$ set equal to zero.

It is then possible to rewrite the state of the master-slave system in function of the formation error:

$$\frac{d}{dt}\begin{bmatrix} e \\ \dot{e} \end{bmatrix} = \begin{bmatrix} \dot{e} \\ \ddot{p}_m - \ddot{p}_s \end{bmatrix} \tag{24}$$

$$= \begin{bmatrix} \dot{e} \\ \frac{1}{M_P}\left(\hat{F}_{D,m} + K_{Pref} e_{ref} + K_{Dref} \dot{e}_{ref} + \hat{M}_P \ddot{p}_{ref} - F_{D,m}\right) - \frac{1}{M_P}(F_s - F_{D,s}) \end{bmatrix}$$

where F_s and $F_{D,s}$ are the magnetic force and drag force related to the slave particle. The master-slave control problem is similar with what carried out before; we need to find a suitable control law F_s such that slave is in formation with the master at every time instant t.

$$F_s = \hat{F}_{D,s} + \frac{1}{M_P}(K_P e_{ref} + K_D \dot{e}_{ref} + \widehat{M}_P \ddot{p}_{ref}) + K_{PS} e + K_{DS} \dot{e} \qquad (25)$$

K_{PS} and $K_{DS} \in \mathbb{R}^{2\times2}$ are the positive definite gain matrices relative to the slave controller, chosen to stabilise the closed-loop master-slave system.

$$\ddot{e} + K_{DS} \dot{e} + K_{PS} e = 0 \qquad (26)$$

The slave PD controller presents the same advantages mentioned before fort the tracking reference control. It worth noting that (25) is linked to the master dynamics not only by the formation error but also taking into account the control input of the master F_{ref}. Moreover, it is important to observe that this control law has been tuned according with its dynamics, and the gains K_{DS} and K_{PS} are different from K_D and K_P.
The simulation results of the master-slave system are shown in section 4.1.2. Figure 12 shows the structure of a whole master-slave system including the two designed controllers.

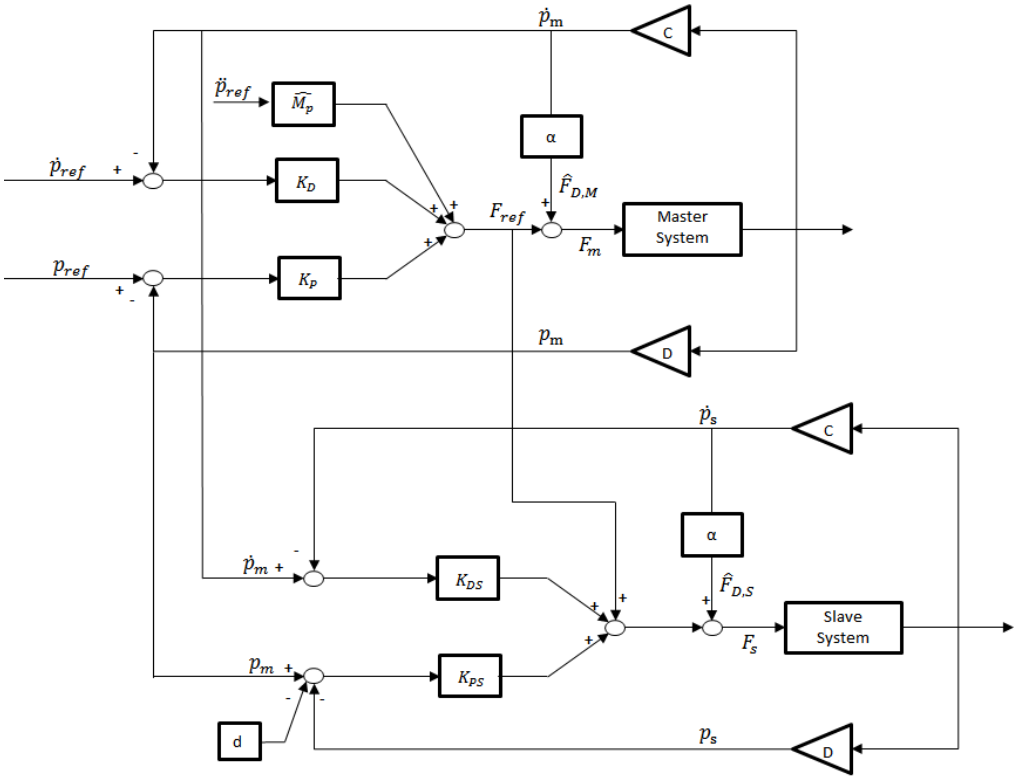

Figure 12-Control scheme of the master-slave control for two microparticles

4.1.3 Formation Control

This chapter is an extension of the previous one to the case of formation tracking control for multiple microrobots.

Let us consider a group of n microrobots with the same dynamics model described beforehand

$$\dot{\xi}_i = A\xi_i + Bf_i(p_i) = \begin{bmatrix} \dot{p}_i \\ \ddot{p}_i \end{bmatrix} = \begin{bmatrix} 0_{2\times2} & I_{2\times2} \\ 0_{2\times2} & \frac{\alpha}{M_p} I_{2\times2} \end{bmatrix} \begin{bmatrix} p_i \\ \dot{p}_i \end{bmatrix} + \begin{bmatrix} 0_{2\times2} \\ \frac{1}{M_p} I_{2\times2} \end{bmatrix} \begin{bmatrix} f_{ix}(p_i) \\ f_{iy}(p_i) \end{bmatrix} \quad (27)$$

with $i \in [1, n]$ the i-th microparticle, characterised by the state of the system ξ_i and input variable $f_i(p_i)$.

The control objective we want to achieve is to make n micro-agents follow the reference trajectory in a straight-line configuration. As it has been mentioned before there is no hetereogeneity between the microparticles. In

this sense everyone can behave as a master either as a slave. The control law able to drive the particle i to the reference position p_{i-1} is given by:

$$\begin{aligned} F_i &= \hat{F}_{D,i} + F_{i-1} \\ &= \hat{F}_{D,i} + \frac{1}{m}(K_P e_{i-1} + K_D \dot{e}_{i-1} + \hat{m}\ddot{p}_{i-1}) + K_{PS} e_i \\ &+ K_{DS} \dot{e}_\iota \end{aligned} \tag{28}$$

Where $F_{i-1}$is the control input which drives the microparticle $i-1$, master of the particle i. e_i represents the formation error between the particle i and the particle $i-1$, i.e. its master, which itself is linked to another particle $i-2$, with the dual law of (25). The two errors are then defined as

$$\begin{aligned} e_i &= p_{i-1} - p_i - d \\ e_{i-1} &= p_{i-1} - p_{i-2} - d \end{aligned} \tag{29}$$

(2) is valid for every particle $i \in [2, n]$. For the microrobots $i = 1$, i.e. the first one which does not follow any particle, the control law (20) holds.
Figure 13 shows the general structure of the decentralised control.

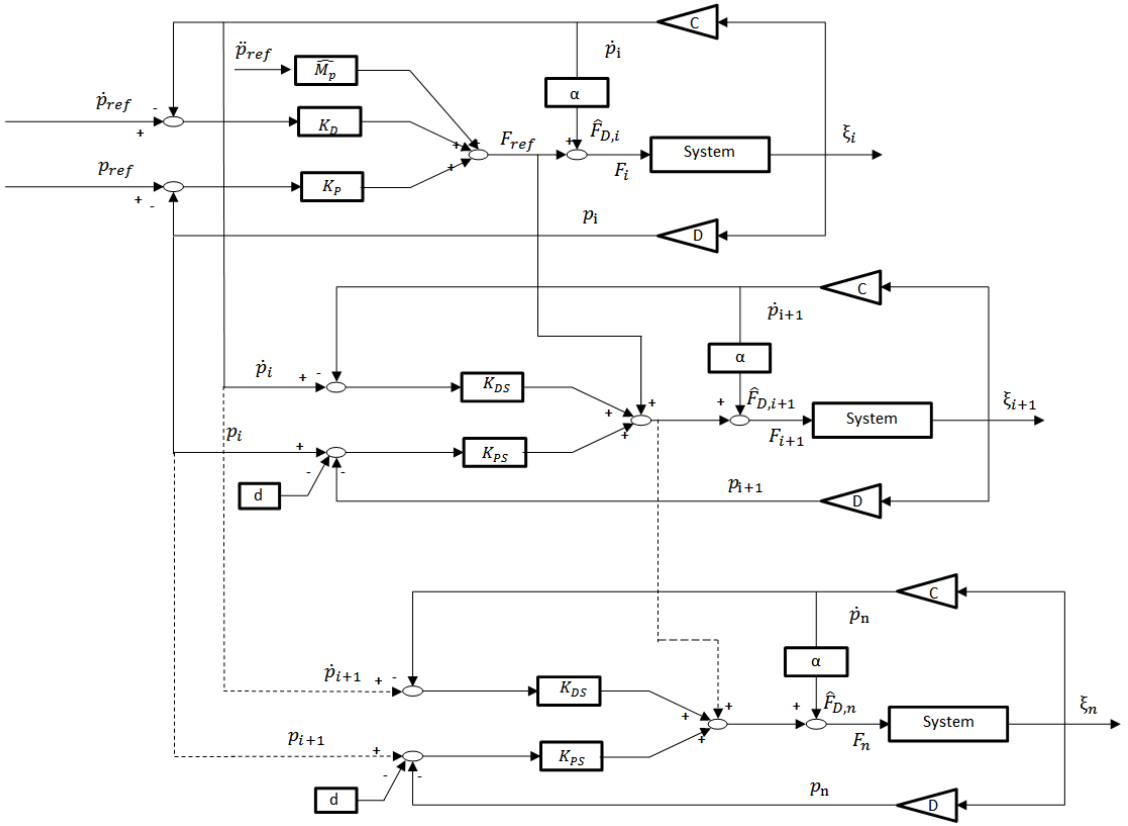

Figure 13-Formation control scheme of multiple microrobots

4.2 Simulation

In order to evaluate the performance of the control laws designed in section 4.1, these have been implemented in Simulink/Matlab and simulated for different trajectories and initial conditions.

4.2.1 Motion Control of Single Microparticles

First, it has been simulated the motion control developed in section 4.1.1. The gain matrices were selected with pole-placement assignment technique. For the design of the controller were chosen two complex conjugate poles $p_{1,2} = -20.46 \pm j2.6 \cdot 10^3$, with a damping factor $\zeta = 0.0078$.
Table 3 shows the constant gain identifying the matrices $K_D = k_d I_{[2\times2]}$ and $K_P = k_p I_{[2\times2]}$.

	$\boldsymbol{k_p}$	$\boldsymbol{k_d}$
Motion Control parameters	$5 \cdot 10^{-3}$	$3 \cdot 10^{-8}$

Table 3. Gain parameters for motion control of a single microparticle

A first test has been carried out by providing to the system a constant signal $\bar{p} = \begin{bmatrix} 0.2 \\ -1 \end{bmatrix}$ [mm] with the initial condition of $\xi_0 = \begin{bmatrix} -0.18\ [mm] \\ 0.18\ [mm] \\ 0 \\ 0 \end{bmatrix}$.
The particle seems to follow precisely the reference trajectory with a rise time around 0.011 seconds.
Figure 14 shows the time response of the given system for the constant signal $\bar{p}$.

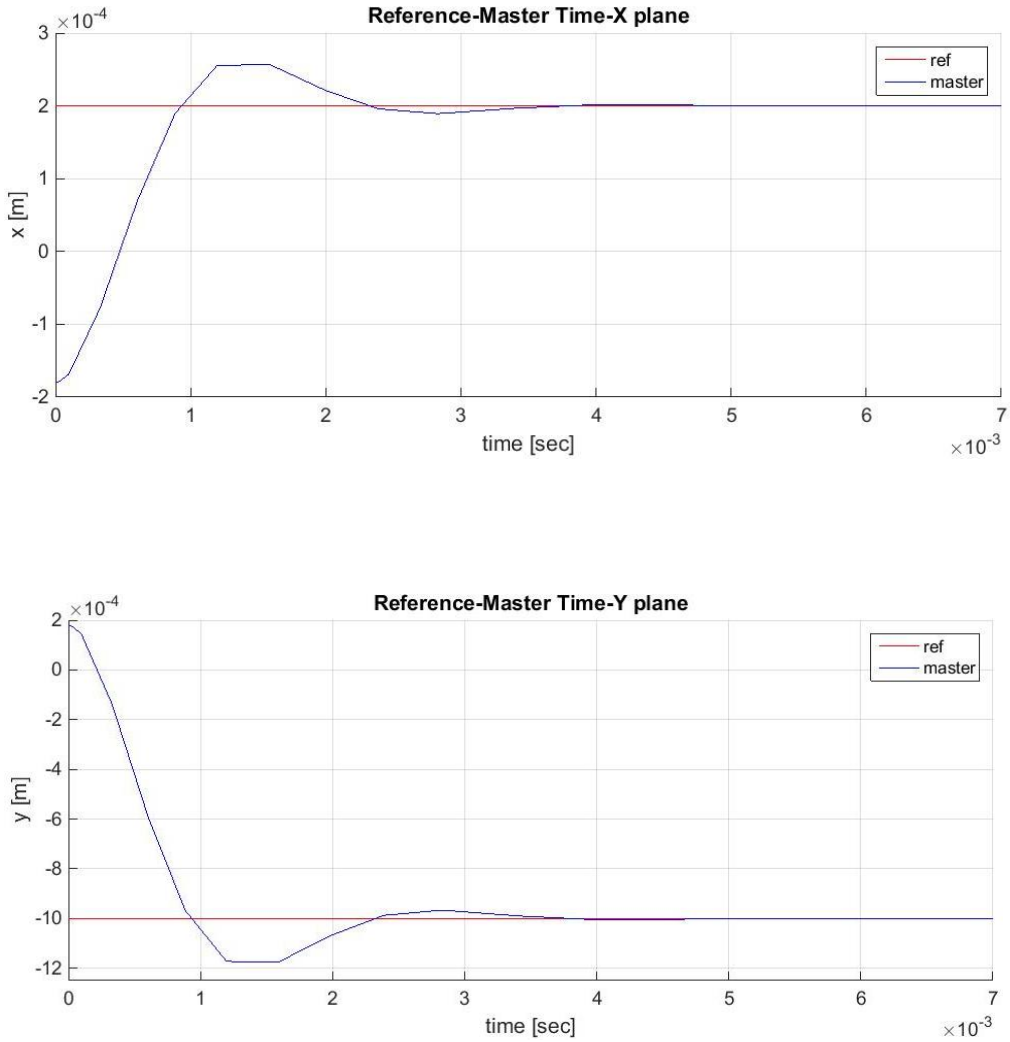

Figure 14-Response time of the system for a step provided as signal input. On the top, it is shown the x vs time response, and the bottom y vs time

The same test has been repeated for a sinusoidal signal with $A = 0.0005$ of amplitude and frequency $f = 10\ Hz$. The performance is reported in Figure 15.

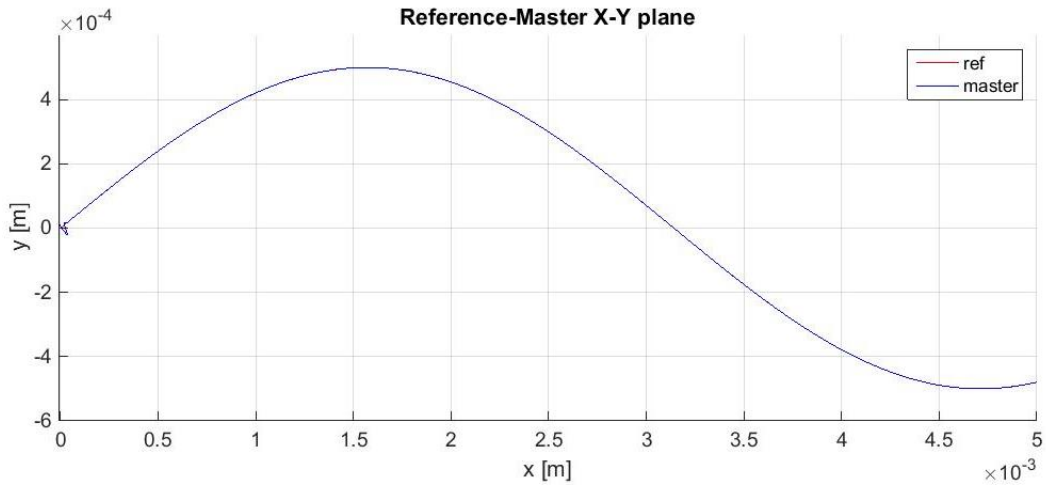

Figure 15- Response time of the system for a sinusoidal reference. X- time response (on the top), Y-time (middle figure) and X-Y plane (on the bottom)

4.2.2 Formation Control

Once the motion control of a single particle has been validated with respect to the reference trajectory we have simulated the Master-Slave Control System with only two microparticles and then extended to three.

The gain matrices $K_{DS} = k_{ds} I_{[2\times2]}$ and $K_{PS} = k_{ps} I_{[2\times2]}$ were tuned with the same pole-placement technique. Although the assigned poles are the same ,the gains differ from the ones computed for tracking control as they have been tuned according to (26), which includes already the contribution of the particle mass. Indeed, $k_{ds} = \frac{k_d}{M_P}$ and $k_{ps} = \frac{k_p}{M_P}$.

Figure 17 reports a simulation with three microparticles. The same sinusoidal input of 4.1.1 has been provided.

Several tests have been done in order to prove the performance of the control, by changing reference input signal and the initial conditions.

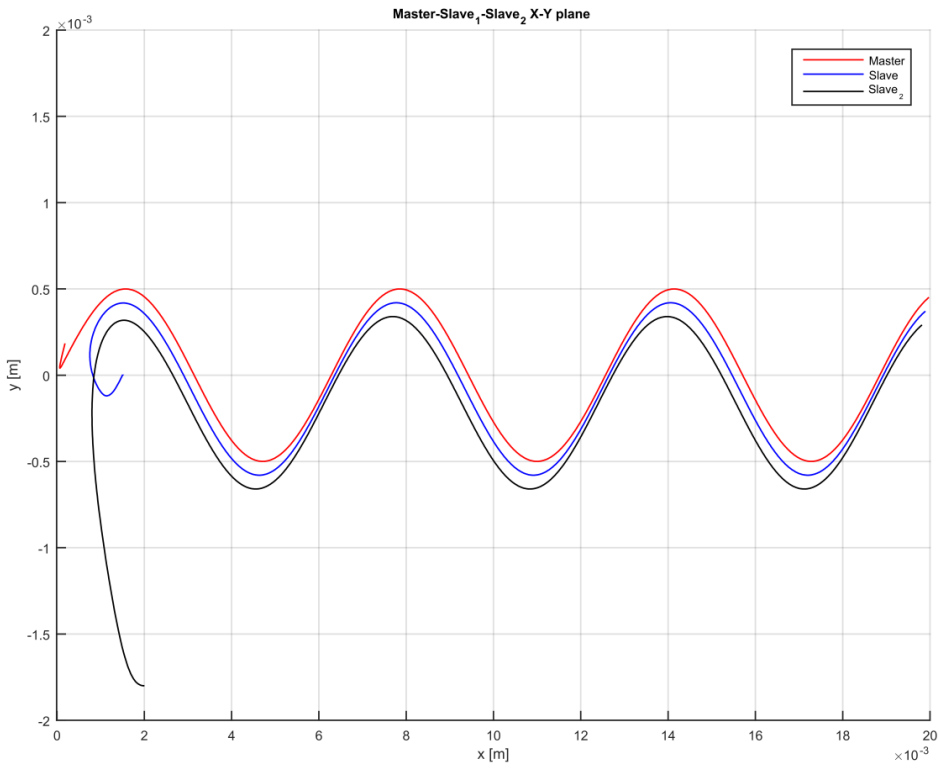

Figure 16-Master-Slave control of three microparticles for a sinusoidal signal

The initial conditions considered for this simulation are indicated in the table below:

	x_0[m]	y_0[m]	$\dot{x}_0$[m/s]	$\dot{y}_0$[m/s]
Master	$-1.8 \cdot 10^{-4}$	$1.8 \cdot 10^{-4}$	0	0
Slave	$1.5 \cdot 10^{-3}$	0	0	0
Slave2	$2 \cdot 10^{-3}$	$-1.8 \cdot 10^{-3}$	0	0

Table 4. Initial conditions of the three microparticles

The three microparticles start all from different initial points of the workspace. In particular the two slaves at the initial time t_0 are out of formation. Thanks to the controller they are forced in formation configuration, kept it for the whole simulation.

Figure 17 and Figure 18, where are reported the formation errors, defined in the form of (29), along with the x and y-direction of the two microparticles in a master-slave configuration. At the beginning of the simulation, the errors are different from zero, as the particles are out of formation, but after 0.2 seconds they reach the straight-line configuration and the formation errors go to zero.

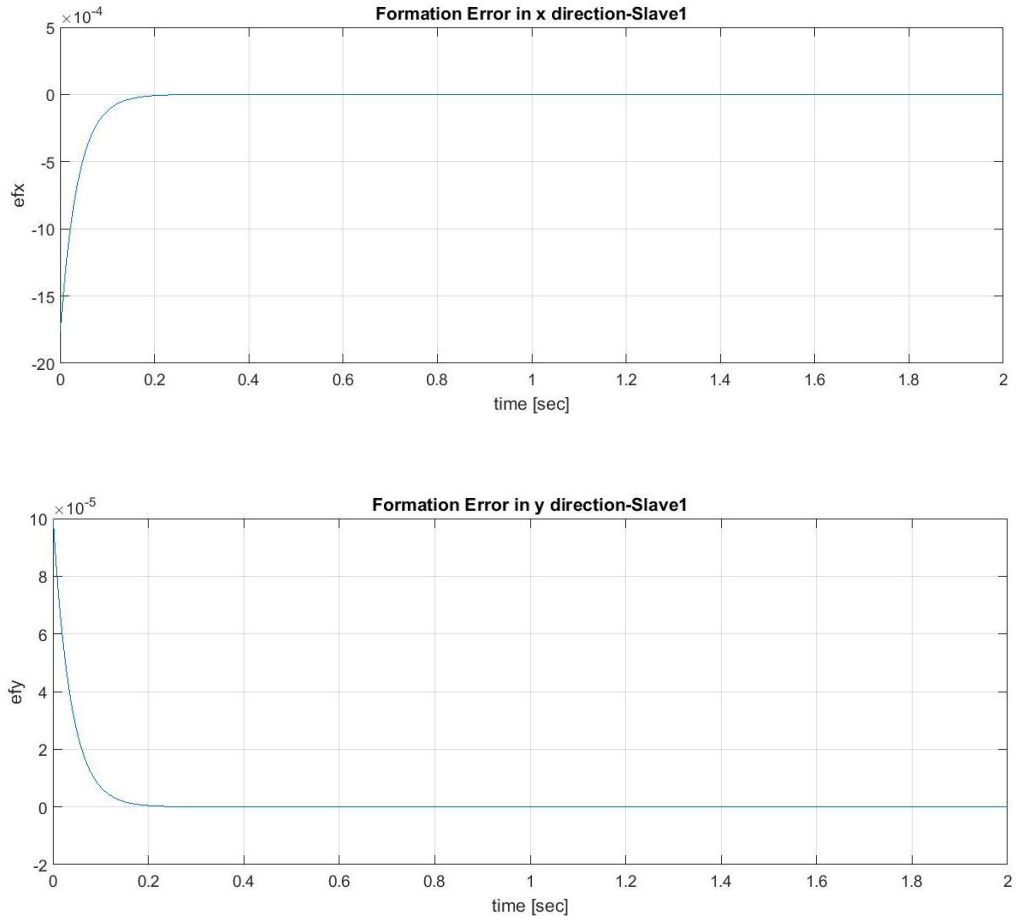

Figure 17-Time response of the formation errors, e_{x_1}(17.a) and e_{y_1}(17. b), of the first slave along x and y direction

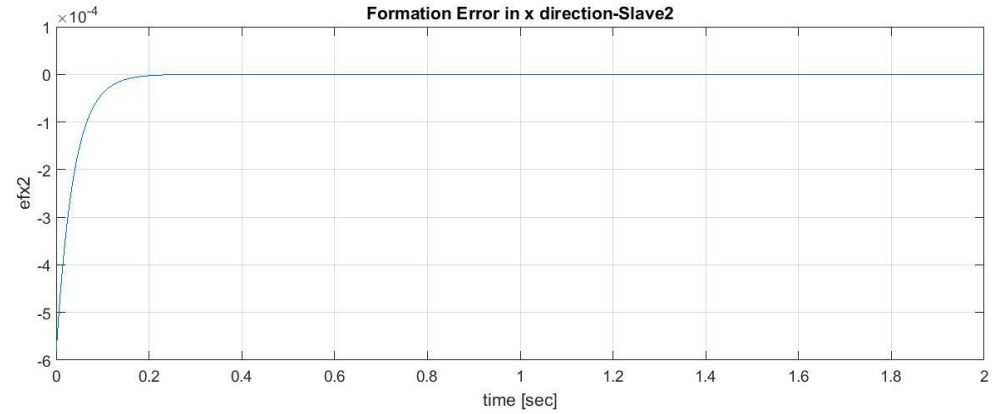

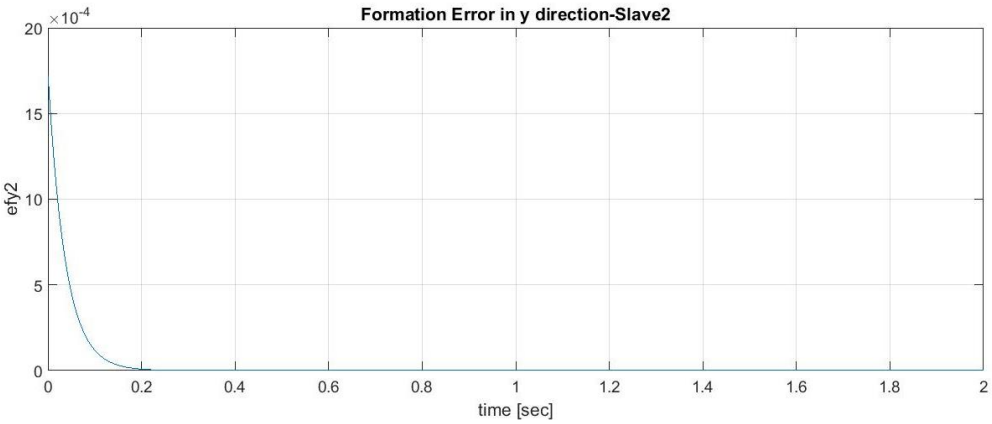

Figure 18-Time response of the formation errors, e_{x_2}(18.a) and e_{y_2}(18.b), of the second slave along x and y direction

Chapter 5
FORCE-TO-CURRENT MAP

The experimental setup described in 3.2 is controllable on the currents. These are responsible for actuating the four electromagnets set at the corners of the workspace. The relation between the current and the magnetic forces, which drive the microparticles along the path, is characterised by a nonlinear function (14). The linear control developed in Chapter 4 assumes as control variable the magnetic force. Indeed, the inversion of the current-to-force nonlinear map has the advantage to simplify the control problem to a linear control design. Assume that an inverse function exists such that

$$g\left(p, g^{-1}(p, \mathrm{F})\right) = F \tag{30}$$

where $g^{-1}(p, \mathrm{F})$ is the current vector for the given position p and the controlled magnetic force F. The inverse mapping problem consists in solving $g^{-1}(\cdot)$ with respect to the currents I, for fixed position $\bar{p} = \begin{bmatrix} x_m \\ y_m \end{bmatrix}$ and given magnetic force $F_m = \begin{bmatrix} F_{mx} \\ F_{my} \end{bmatrix}$, provided by the controller.

The system presents $n = 4$ unknowns, i.e. the four currents $I = [I_1 \quad I_2 \quad I_3 \quad I_4]^T$ actuating the electromagnets, and only two equations:

$$\begin{cases} F_{mx} = \beta\, I^T \dfrac{\partial}{\partial x}\left(\tilde{B}(x_m, y_m)^T\, \tilde{B}(x_m, y_m)\right) I \\ F_{my} = \beta\, I^T \dfrac{\partial}{\partial y}\left(\tilde{B}(x_m, y_m)^T\, \tilde{B}(x_m, y_m)\right) I \end{cases} \tag{31}$$

with β the coefficient defined in 3.3.

The problem was firstly tackled by adopting an analytical approach (M.A) according to a theory which is proposed in [29]. As the results obtained by the M.A turned out to be unsatisfying, an optimisation approach was, successively, implemented.

Both approaches have been tested and compared. Finally, the inverse map achieved thanks to the optimisation technique has been integrated with the tracking control of one microparticle. Simulations are provided in the last paragraph.

5.1 One Particle: Comparison of the Analytical and Optimisation Methods

5.1.1 M.A. Method

In the previous section, the magnetic force is defined as a quadratic function depending on the magnetic field. This varies with the currents and the position. So, in this regard, (14) can be written as the gradient with respect to the p of the square Euclidian norm of the magnetic field:

$$F_m(p, I) = \beta \nabla \left|\left|B(p, I)\right|\right|^2 = \beta \boldsymbol{g}(\boldsymbol{p}, \boldsymbol{I}) \tag{32}$$

with $g(\cdot) : \mathbb{R}^2 \times \mathbb{R}^4 \rightarrow \mathbb{R}^2$.

As the coils operate in their linear regime, the magnetic field varies linearly with the current and it can be written as (10). Thus, substituted in (32), and computed the gradient with respect to p, it yields:

$$g(p, I) = \nabla \left|\left|\tilde{B}(p) I\right|\right|^2 = 2 \left[\frac{\partial(\tilde{B}(p) I)}{\partial p}\right]^T \tilde{B}(p) I \tag{33}$$

with $\partial \tilde{B}(p) I / \partial p$ the Jacobian matrix of the magnetic field $B(p, I)$.

Let us define a parametric variable r such that

$$\tilde{B}(p)I = r \tag{34}$$

Firstly,(34) was multiplied both sides by r^T and then differentiated by p.

$$2\left[\frac{\partial \tilde{B}(p)I}{\partial p}\right]^T r = 2\left[\frac{\partial (\tilde{B}^T(p)r)}{\partial p}\right]^T I = F_m \tag{35}$$

By merging (34) and (35), for a fixed value of the vector parameter r, a linear equation with respect to I in the form of Ax=B is obtained:

$$\begin{bmatrix} \tilde{B}(p) \\ \left(\frac{\partial (\tilde{B}^T(p)r)}{\partial p}\right)^T \end{bmatrix} I = \begin{bmatrix} r \\ \frac{1}{2}F_m \end{bmatrix} \tag{36}$$

Defining the polar representation of the parameter $r = \rho[cos\varphi \quad sin\varphi]^T$, with $\rho > 0$ and $\varphi \in [0,2\pi)$, and substitute in (36) and left multiplying by suitable non-singular matrix, the equation can be rewritten as:

$$H(\varphi)\tilde{B}_e(p)I = \rho e_1 + \frac{1}{2}[e_3\ e_4]F_m \tag{37}$$

where $e_i \in \mathbb{R}, i = 1,3,4$ is a vector of 0 elements except with a 1 at row i. The non-singular matrix $H(\varphi) \in \mathbb{R}^{n\times 5}$ is given by:

$$H(\varphi) = \begin{bmatrix} cos\varphi & sin\varphi & 0 & 0 & 0 \\ -sin\varphi & cos\varphi & 0 & 0 & 0 \\ 0 & 0 & cos\varphi & sin\varphi & 0 \\ 0 & 0 & 0 & cos\varphi & sin\varphi \end{bmatrix} \tag{38}$$

while $\tilde{B}_e(p)$ is a $5\times n$ matrix:

$$\tilde{B}_e(p) = \begin{bmatrix} \tilde{B}(p) \\ \frac{\partial \tilde{B}(p)}{\partial x\tilde{B}(p)} \\ \frac{\partial([0\ 1]\tilde{B}(p))}{\partial y} \end{bmatrix} = \begin{bmatrix} \tilde{B}(p) \\ \frac{\partial([0\ 1]\tilde{B}(p))}{\partial x} \\ \frac{\partial \tilde{B}(p)}{\partial y} \end{bmatrix} \tag{39}$$

This equality is due to Maxwell's equation $\nabla\times B = \frac{1}{c^2}\frac{\partial E}{\partial t}$. Indeed, under the hypothesis of constant electric field in the region of interest, (40) is obtained.

$$\frac{\partial([0 \quad 1]\tilde{B}(p))}{\partial x} = \frac{\partial([1 \quad 0]\tilde{B}(p))}{\partial y} \tag{40}$$

Thanks to this method the system has been reduced to a linear system of 4 unknowns in 4 equations. Thus, if a solution of (37) exists, it is unique and it can be computed by left multiplying both sides of the equation by the inverse of $H(\varphi)\tilde{B}_e(p)$:

$$I = (H(\varphi)\tilde{B}_e(p)^{-1}(\rho e_1 + \frac{1}{2}[e_3 \; e_4]F_m) \tag{41}$$

5.1.2 Optimization Algorithm

An optimisation method characterised by finite approximation of gradient and hessian functions (GHA), was adopted as the second attempt to solve the inversion problem.

Let us consider an interior-point optimisation:

$$\begin{aligned} &\text{minimize } f_0(x) \\ &\text{subject to } f_{in_i}(x) \leq 0, i = 1, \dots, m \\ &h_i(x) = 0, i = 1, \dots, p \end{aligned} \tag{42}$$

where x represents the optimization variable that minimizes the cost function $f_0(x)$, according to the inequality constraints $f_{in_i}(x) \leq 0,\ i = 1, \dots, m$, and equality constraints $h_i(x) = 0, i = 1, \dots, p$.

For our case-study, the electrical power has been chosen as a cost function, minimised with respect to the current vector. Assume as inequality constraint the saturation element due to the limitation of Elmo's drives $I \in [-I_{max}, I_{max}]$, while the algebraic equations (31), related to the magnetic control forces as the strict equality constraint:

$$\begin{aligned} f_0(I) &= \frac{1}{2} I^T I \\ f_{in}(I) &= \begin{bmatrix} -I - I_{max} \\ I - I_{max} \end{bmatrix} \end{aligned} \tag{43}$$

$$h(I) = F_m - \beta\, I^T \nabla(\tilde{B}(p)^T \tilde{B}(p))I$$

with F_m is the magnetic force which the tracking controller outputs. To solve the optimisation, we have used the function *fmincon* of Matlab, which find the minimum of constrained nonlinear multivariable function.

As the microparticle system deals with small numbers, close to zero, the finite approximation of the derivatives computed by the Matlab toolbox can cause numerical errors. For this reason, the algorithm was improved by providing the analytical forms of the gradient and the hessian (GHP) [20, 21].

5.1.3 Evaluation procedure of the M.A and Optimization approaches

Both approaches were implemented in Matlab and tested on the whole workspace with the following procedure:

- Let us assume to feed the electromagnets with arbitrary currents $\bar{I}$. This set of currents generate a magnetic field. By using the model implemented before it is possible to compute the magnetic force $\bar{F}$ in every point of the workspace $\bar{p}$
- When providing the magnetic force $\bar{F}$ and the actual position, the inverse map outputs the currents, which are able to generate, in that position of the workspace, the required magnetic force in order to move the particle towards the reference trajectory
- The magnetic force F_{InvMap} is now computed according to the currents provided by the inverse map.
- The two forces, computed at the initial step and in the final one, are compared in order to understand which approach is more accurate.

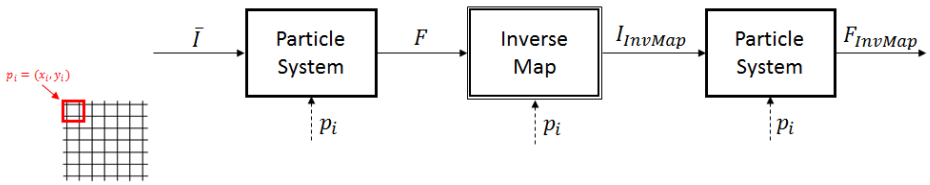

Figure 19-General logic to evaluate the accuracy of the inversion approaches proposed

The procedure has been repeated for every point of the workspace and with different initial currents. The approaches have been evaluated through the magnetic forces as we are not interested in obtaining the same combination of current, but one able to generate the exact components of the force required to compute the desired motion.

The optimisation method, in particular, GHP, seems to compute a more accurate inversion of the map. Thus it has been implemented in Simulink and tested with the whole system, including the motion control.

The results are shown in section 5.3.

5.2 GHP Algorithm applied to Two Particles case

This section focusses on the inversion problem for two microparticles, in order to apply the Master-Slave control developed in section 4.1.2.

The inversion problem slightly differs from the one described before as, in this case, $g(\cdot)$ takes into account also the magnetic force and the position of the slave.

$$g\left(p_m, p_s, g^{-1}(p_m, p_s, F_m, F_s)\right) = [F_m \; F_s]^T \qquad (44)$$

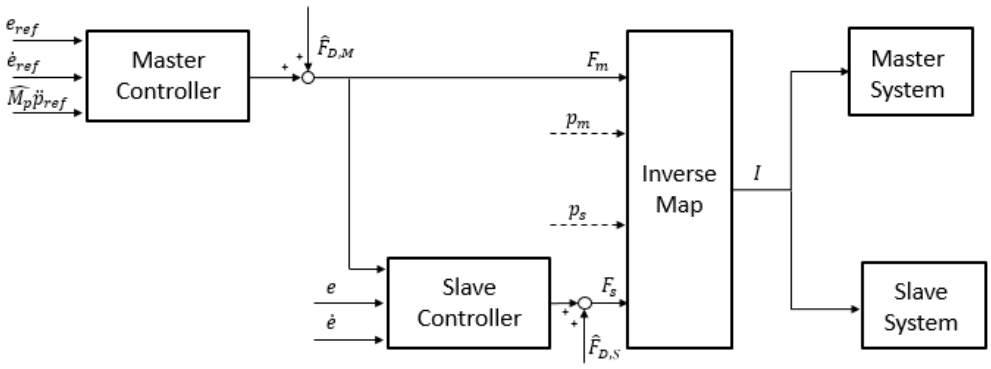

Figure 20-Inverse Mapping for two microparticles

It is worth observing that now the four currents are required to satisfy the constraints related to two microparticles.

The objective function and the inequality constraint $g(I)$ remain the same of (43). On the contrary, the equality constraint $h(I) \in \mathbb{R}^{4\times1}$includes the slave contribution too and can be written as:

$$h(I) = \begin{cases} F_{mx} - \beta\, I^T \dfrac{\partial}{\partial x}\left(\tilde{B}(x_m, y_m)^T\, \tilde{B}(x_m, y_m)\right) I = 0 \\ F_{my} - \beta\, I^T \dfrac{\partial}{\partial y}\left(\tilde{B}(x_m, y_m)^T\, \tilde{B}(x_m, y_m)\right) I = 0 \\ F_{sx} - \beta\, I^T \dfrac{\partial}{\partial x}\left(\tilde{B}(x_s, y_s)^T\, \tilde{B}(x_s, y_s)\right) I = 0 \\ F_{sy} - \beta\, I^T \dfrac{\partial}{\partial y}\left(\tilde{B}(x_s, y_s)^T\, \tilde{B}(x_s, y_s)\right) I = 0 \end{cases} \tag{45}$$

The algorithm was evaluated by the same procedure followed for one microparticle. Several tests have been done by changing the initial condition of the currents and the tolerances.

The optimisation technique does not seem to be able to find a solution which can satisfy the constraints.

The unsuccessful results moved us backwards to inquire whether a solution exists. For this, it can be useful to formulate the problem from an algebraic point of view.

Assume each equation of the system (45) structured in the form of $C = X^T AX$, where:

- $C = \frac{F_{i,j}}{\beta} \in \mathbb{R}$, with $F_{i,j}$ is the $j = x, y$ component of the magnetic force of the i-th microparticle
- $X = I = \begin{bmatrix} I_1 \\ I_2 \\ I_3 \\ I_4 \end{bmatrix} \in \mathbb{R}^{4\times1}$
- $A = \frac{\partial}{\partial j}\left(\tilde{B}(x,y)^T\, \tilde{B}(x,y)\right) = \begin{bmatrix} a & b & c & d \\ b & e & f & g \\ c & f & h & i \\ d & d & i & j \end{bmatrix} \in \mathbb{R}^{4\times4}$

The matrix A is symmetric and its element change with the position.
Suppose we keep constant one current in order to reduce the variables of the system. Therefore, each equation can be seen as a second-order algebraic surface.
The solution of the inverse problem consists in finding the intersections of the four quadric surfaces if these exist.

Unfortunately, in nonlinear equations, the existence and uniqueness of solutions are not guaranteed as in the linear domain.
Due to the difficulty, the problem represents still an open issue, which has to be studied and tackled in the future.

5.3 Simulation

In this chapter, some results of the inversion techniques discussed in paragraph 5.1 are shown.
Several tests were carried out with different arbitrary currents. Here a simulation is reported with only one coil activated $I = [0 \quad 0.5 \quad 0 \quad 0]^T$[A] and the initial currents equal to $I_0 = [0 \quad 0 \quad 1e^{-16} \quad 0]^T$[A].

In Table 5 are reported respectively the minimum, maximum and mean absolute error of the magnetic forces along the x and y-direction.

	$\boldsymbol{min(E_X)}$ [N]	$\boldsymbol{Max(E_X)}$ [N]	$\boldsymbol{\bar{E}_X}$ [N]	$\boldsymbol{min(E_Y)}$ [N]	$\boldsymbol{Max(E_Y)}$ [N]	$\boldsymbol{\bar{E}_Y}$ [N]
M.A	$3.75e^{-17}$	$1.23e^{-08}$	$1.23e^{-08}$	$4.68e^{-16}$	$2.38e^{-08}$	$1.77e^{-09}$
GHA	0	$7.25e^{-09}$	$6.65e^{-10}$	0	$2.25e^{-08}$	$5.33e^{-10}$
GHP	0	$1.07e^{-08}$	$1.79e^{-10}$	0	$2.28e^{-08}$	$3.01e^{-10}$

Table 5. Minimum, maximum and mean values of the absolute errors related to the component of the magnetic forces in x and y-direction. The values have been computed for the three techniques

Clearly, the analytic method (M.A) presents the worst results, not being able to reproduce the intense magnetic forces close to the coil which is activated. On the other hand, the optimisation methods seem to obtain positive results in term of accuracy of the inverse mapping for one microparticle. In particular, it is worth noticing how the GHP has better performance with respect to GHA (see Figure 21).

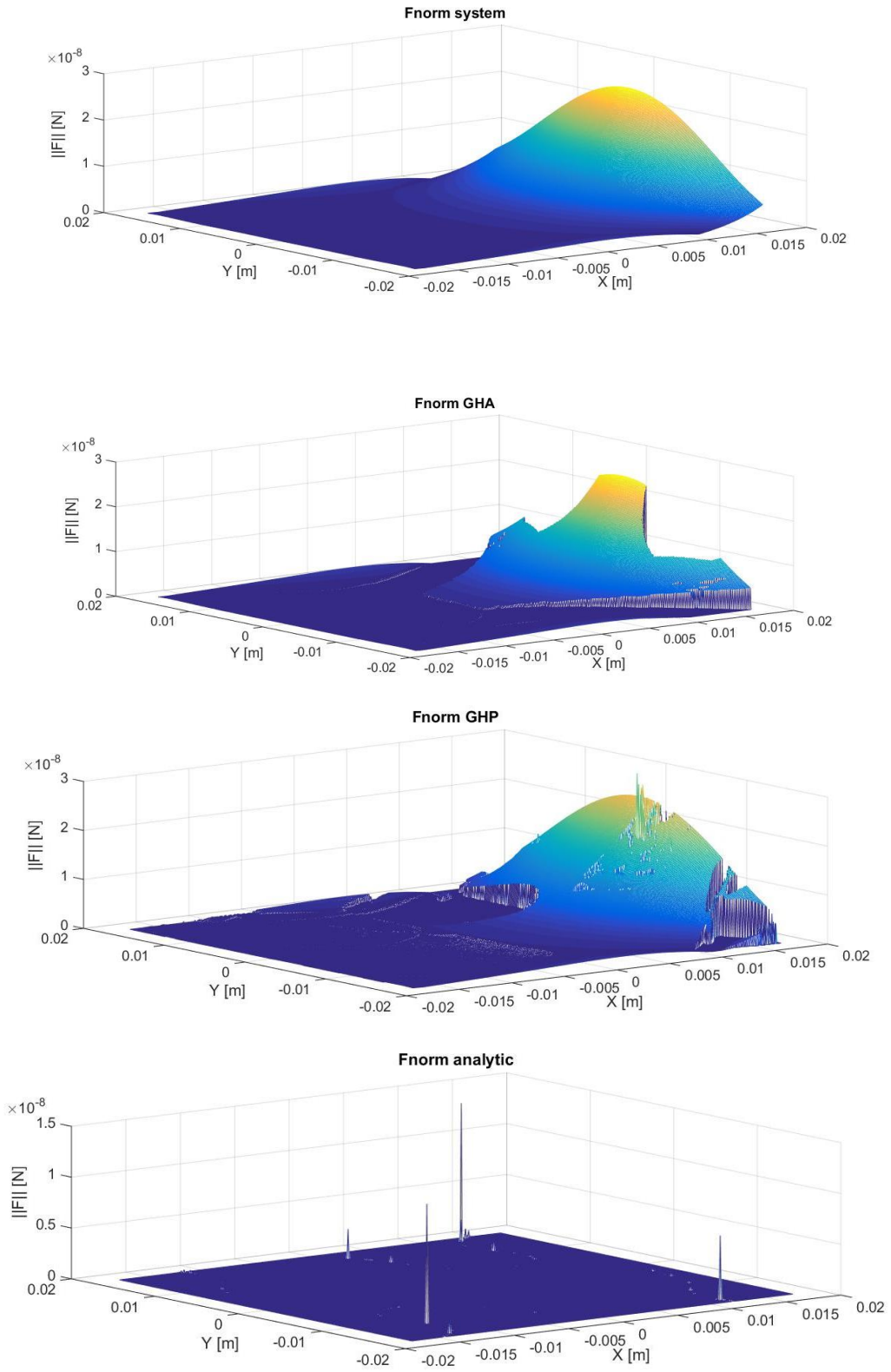

Figure 21-Norm of the magnetic force computed by the simulation model (21.a), GHA algorithm (21.b), GHP algorithm (21.c), M.A method (21.d)

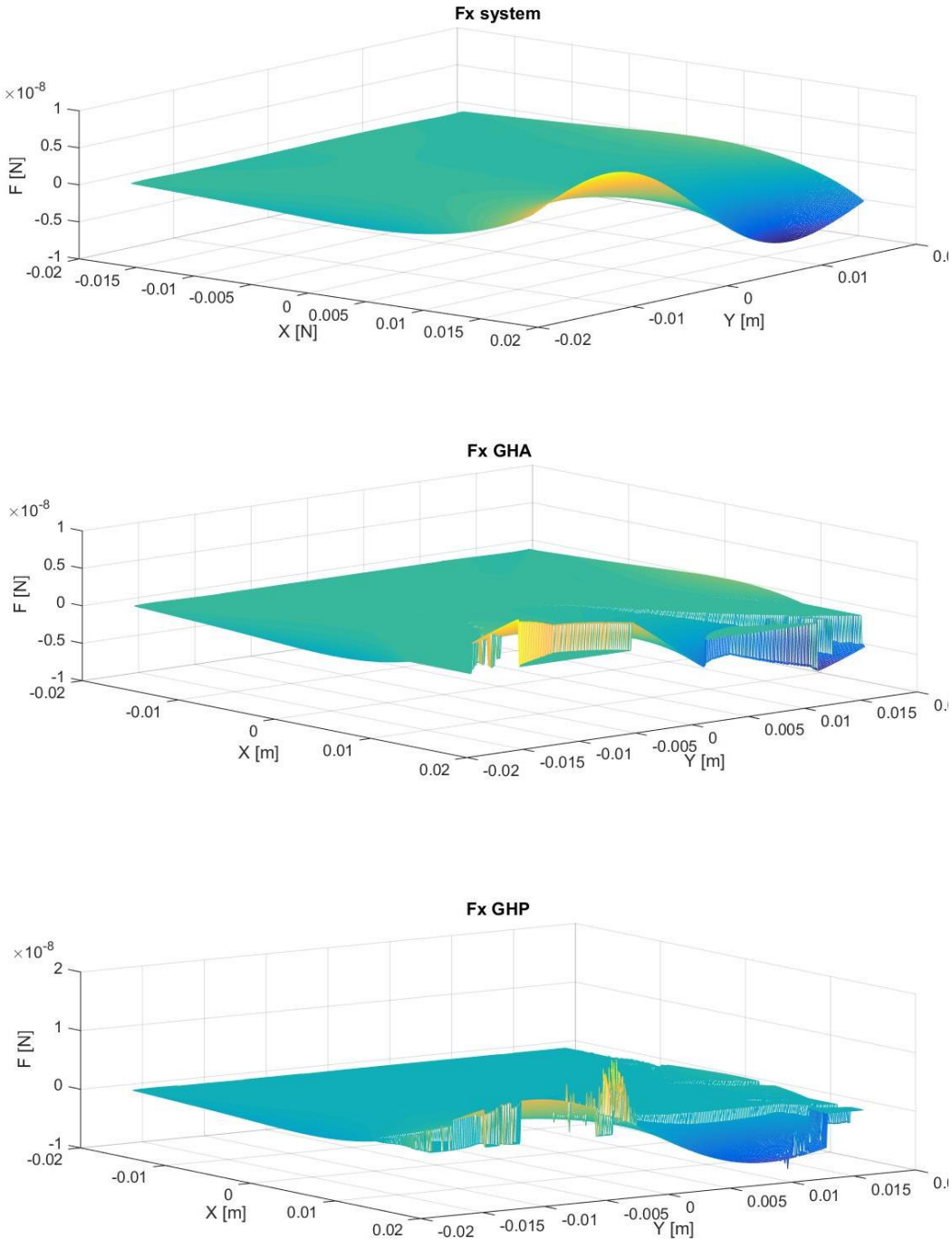

Figure 22- x-component of the magnetic force computed by the simulation model (22.a), GHA algorithm (22.b), GHP algorithm (22.c)

The inverse map, given by the GHP algorithm, was implemented in Simulink and integrated with the overall simulation model, including the tracking control of section 4.1.1.

In Figure 23Figure 24 the tracking of a microparticle to reference point $\bar{p} = (1.5e^{-4}, 2e^{-4})$ is shown, starting from the initial position $p_0 = (0, 0)$, at zero speed.

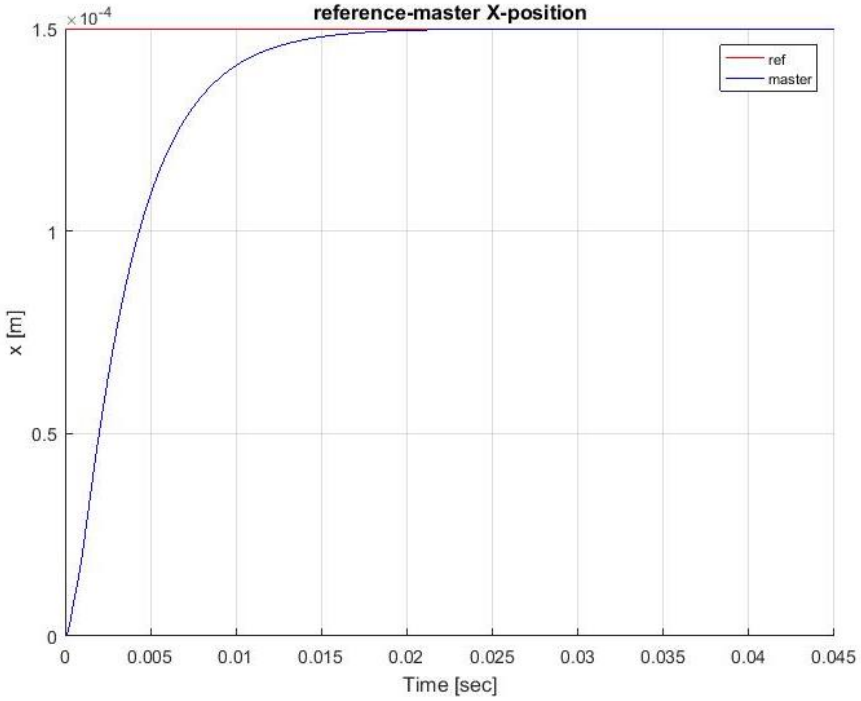

Figure 23- Response time of the system for a constant reference trajectory in x direction

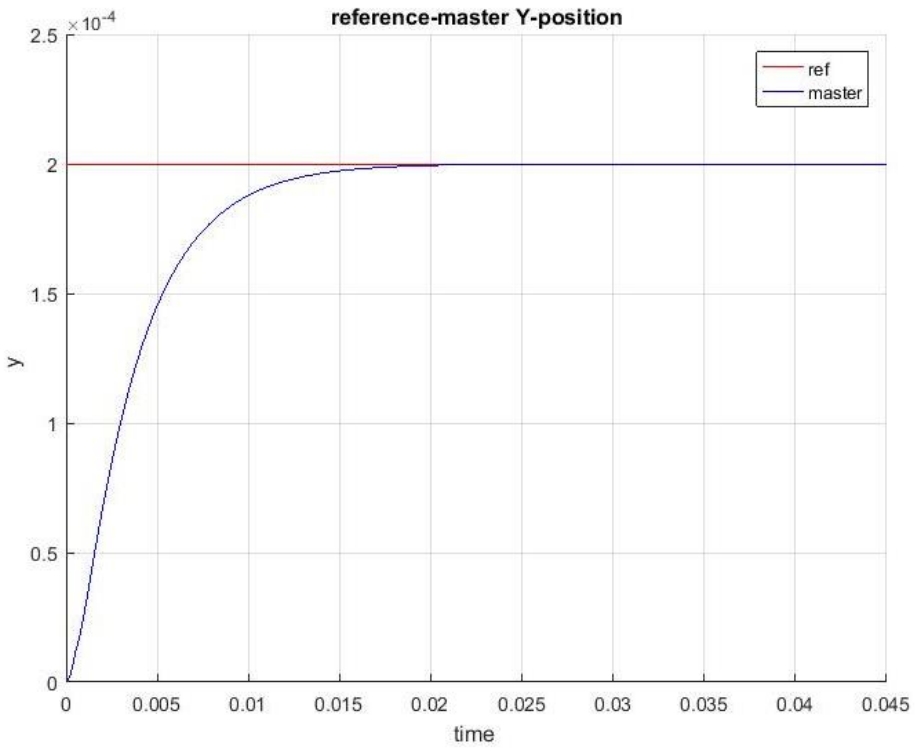

Figure 24- Response time of the system for a constant reference trajectory in y direction

The tracking performance of the microparticle is good, but due to the computational power required by the optimisation algorithm, the overall system is slowly.

In Figure 25 the dynamics of the currents during the simulation can be observed. The four currents are characterised by step-wise changes as the optimisation technique chooses the current vector which minimises the electrical losses, without considering the damage that these oscillations can cause to the setup.
Chapter 6 will suggest a possible solution prevent this behaviour of the currents

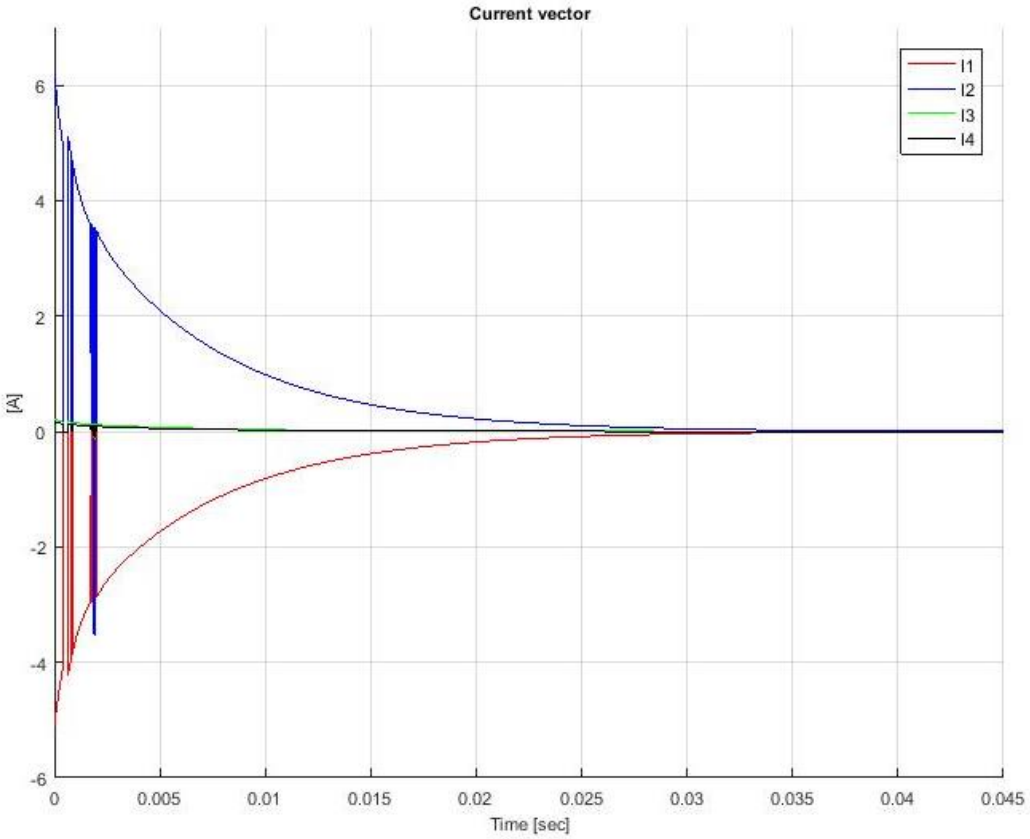

Figure 25- Response time of the four currents during the tracking trajectory control

Chapter 6

CONCLUSION AND FUTURE WORKS

Micro-sized robots have the potential to play a crucial role in health care. However, the goal of precisely controlling the trajectory of microparticles through the human vascular system still needs to be accomplished in order to enable applications such as minimally invasive surgery and targeted drug delivery.

In this work, a feedback motion control for paramagnetic microparticles is presented. A model of the overall magnetic system has been developed according to the experimental setup and the paramagnetic microparticle. In particular, through input/output linearization the nonlinear control problem can be simplified into a linear position/force controller and a nonlinear contribution, given by the force-to-current map. The motion control has been designed with a pole-placement technique in order to stabilise the system. Furthermore, a tracking control for two microparticles in master-slave configuration is proposed. It has then been extended to multiple microrobots for a preliminary study of formation control.
An optimisation algorithm has been developed and compared with an analytical approach provided by the literature. Simulation results are provided for evaluating the performance of the designed control.

The controller performs well for single microparticles that track their reference position, even if the control of several particles proved to be challenging, due to the nonlinear force-to-current relationship/mapping. The optimisation algorithm, however, still leads to a considerable computation time, and the resulting currents show a discontinuous behaviour, which can potentially damage the experimental setup.

Several aspects of this work have been identified for future studies, and can be investigated in order to improve position control and accomplish formation control of multiple microrobots:

- A filter to prevent the discontinuities of the currents' dynamics has to be implemented. In [29] a nonlinear filter it is shown.
- In order to apply formation control on the experimental setup, as proposed in this thesis, the problem of the force-to-current map for the case of multiple microrobots needs to be solved(/addressed).
- According to Mobimag setup, only the particle's positions are directly measurable. A set of three observers is required in order to estimate the remaining state variables and to obtain information on the velocities. More details can be found in [27].

Bibliography

[1] B. J. Nelson, “Microrobotics in Medicine.” .

[2] S. Henry and M. D. Cabin, *The Heart and Circulation*. William Morrow & Co., 1992.

[3] Baldissera, Grassi, Negrini, and Porro, *Fisiologia e biofisica medica*, vol. 1,2. Poletto, 2009.

[4] Martel, S., “Magnetic Navigation Control of Microagents in the Vascular Network,” *IEEE CONTROL Syst. Mag.*, Dec. 2013.

[5] K. K. Jain, “Editorial: Targeted drug delivery for cancer,” *Technol Cancer Treat*, vol. 4, no. 4, pp. 311–313, 2005.

[6] M. Sitti, H. Ceylan, W. Hu, and E. Diller, “Biomedical Applications of Untethered Mobile Milli/Microrobots,” *Proc. IEEE*, Feb. 2015.

[7] Abbott J., Nagy J., Beyeler F., and Nelson B., “Robotics in the small,” *IEEE Autom Mag*, 2007.

[8] Federico Carpi and Carlo Pappone, “Magnetic Manoeuvring of Endoscopic Capsules by Means of a Robotic Navigation System,” *5*, vol. 56, May 2009.

[9] S. Martel *et al.*, “Mri-based medical nanorobotic platform for the control of magnetic nanoparticles and flagellated bacteria for target interventions in human capillaries,” *Int J Robot Res*, no. 28(9), pp. 1169–1182, 2009.

[10] S. Martel, J-B. Mathieu, O. Felfoul, and A. Chanu, “Automatic navigation of an untethered device in the artery of a living animal using a conventional clinical magnetic resonance imaging system,” *Appl Phys Lett*, no. 90(11), 2007.

[11] C. Pawashe, S. Floyd, and M. Sitti, “Modelling and experimental characterization of an untethered magnetic micro-robot.,” *Int J Robot Res*, no. 28(8), pp. 1077–1094, 2009.

[12] E. Diller, S. Floyd, C. Pawashe, and M. Sitti, “Control of multiple heterogeneous magnetic microrobots in two dimensions on non-specialized surfaces.,” *IEEE Trans Robot*, no. 28(1), pp. 172–182, 2012.

[13] K. Cheang U, K. Lee, AA. Julius, and MJ. Kim, “Multiple-robot drug delivery strategy through coordinated teams of microswimmers,” *Appl Phys Lett*, vol. 105(8), no. 83705, 2014.

[14] Cappelleri D., Efthymiou D., Goswami A., Vitoroulis N, and Zavlanos M, “Towards mobile microrobot swarms for additive microfacturing,” *Int J Adv Robot Syst 11 150*, 2014.

[15] N. A. Torres and D. O. Popa, “Cooperative Control of Multiple Untethered Magnetic Microrobots Using a Single Magnetic Field Source,” *IEEE Int. Conf. Autom. Sci. Eng. CASE*, Aug. 2015.

[16] Michael P. Kummer, Jake J. Abbott, Bradley E. Kratochvil, Ruedi Borer, and Bradley Nelson, “OctpMag: An Electromagnetic System for 5-DOF Wireless Micromanipulation,” *6*, vol. 26, Dec. 2010.

[17] Alper Denasi and Sarthak Misra, “A Robust controller for microsized agents-The prescribed performance approach,” presented at the in Proceedings of the Annual International Conference on Manipulation, Automation, and Robotics at Small Scales (MARSS), 2016.

[18] D. R. Nelson, D. B. Barber, and T. W. McLain, “Vector field path following for small unmanned air vehicles,” presented at the in Proc. American Control Conference, 2006.

[19] F. Ongaro, S. Scheggi, C. Yoon, F. van den Brink, S. Hyun Oh, and S. Misra, “Autonomous planning and control of soft untethered grippers in unstructered enviroments,” *J Micro-Bio Robot*, Aug. 2016.

[20] F. Ongaro, C. Pacchierotti, C. Yoon, D. Prattichizzo, D. H. Gracias, and S. Misra, “Evaluation of an Electromagnetic System with Haptic Feedback for Control of Untethered, Soft Grippers Affected by Disturbances,” presented at the International Conference on Biomedical Robotics and Biomechatronics (Biorob), 2016.

[21] H. Khalil, *Nonlinear Systems*, Third Edition. Prentice Hall, 2002.

[22] M. A. Henson and D. E. Seborg, *Nonlinear Process Control*. Prentice Hall, 1997.

[23] P. Bolzern, R. Scattolini, and N. Schiavoni, *Fondamenti di Controlli Automatici*, Seconda Edizione. McGraw-Hill, 2004.

[24] L. Magni and R. Scattolini, *Advanced and Multivariable Control*. Pitagora editrice Bologna.

[25] K. Ogata, *Modern Control Engineering*. 1970.

[26] Khalil Islam S. M. and Misra Sarthak, "Magnetic-Based Motion Control of Paramagnetic Microparticles With Disturbance Compension," *IEEE TRANSACTIONS*, vol. 50, no. 10, Oct. 2014.

[27] H. Nijmeijer and A. Rodriguez-Angeles, *Synchronization of Mechanical Systems*, vol. 46. World Scientific.

[28] I. I. Blekhman, A. L. Fradkov, H. Nijmeijer, and A. Yu. Pogromsky, "On self-synchronization and controlled synchronization," *Systems & Control Letters - Special issue: Control of chaos and synchronization*, vol. 31, no. 5, pp. 299–305, Oct. 1997.

[29] A. Komaee and B. Shapiro, "Steering Ferromagnetic Particle by Optimal Magnetic Feedback Control," *IEEE TRANSACTIONS ON CONTROL SYSTEMS TECHNOLOGY*, 2011.

[30] P. Y. Papalambros and D. J. Wilde, *Principles of Optimal Design*, Second edition. University of Cambridge.

[31] https://nl.mathworks.com/help/optim/ug/writing-scalar-objective-functions.html#bu2w6a9-1, *Matlab*. .